Title: Discovery of a molecular glue that enhances UPR^{mt} to restore proteostasis *via* TRKA-GRB2-EVI1-CRLS1 axis

Authors: Li-Feng-Rong Qi[1, 2 †], Cheng Qian[1, †], Shuai Liu[1, 2†], Chao Peng[3, 4], Mu Zhang[1], Peng Yang[1], Ping Wu[3, 4], Ping Li[1] and Xiaojun Xu[1, 2 *]

† These authors share joint first authorship

Running title: Ginsenoside Rg3 reverses Parkinson's disease model by enhancing mitochondrial UPR

Affiliations:

1 State Key Laboratory of Natural Medicines, China Pharmaceutical University, 210009, Nanjing, Jiangsu, China.

2 Jiangsu Key Laboratory of Drug Discovery for Metabolic Diseases, China Pharmaceutical University, 210009, Nanjing, Jiangsu, China.

3. National Facility for Protein Science in Shanghai, Zhangjiang Lab, Shanghai Advanced Research Institute, Chinese Academy of Science, Shanghai 201210, China

4. Shanghai Science Research Center, Chinese Academy of Sciences, Shanghai, 201204, China.

Corresponding author:

Ping Li, State Key Laboratory of Natural Medicines, China Pharmaceutical University, 210009, Nanjing, Jiangsu, China. Email: liping2004@126.com,

Xiaojun Xu, State Key Laboratory of Natural Medicines, Jiangsu Key Laboratory of Drug Discovery for Metabolic Diseases, China Pharmaceutical University, 210009, Nanjing, Jiangsu, China. Telephone number: +86-2583271203, E-mail: xiaojunxu2000@163.com.

Abstract

Lowering proteotoxicity is a potentially powerful approach for the treatment of neurological disorders, such as Parkinson's disease. The unfolded protein response (UPR) is a major mechanism that preserves the network maintaining cellular proteostasis. In the present study, we developed the screening strategy to discover compounds that significantly enhanced the activation of mitochondrial UPR (UPR^{mt}) through increasing cardiolipin content. We identified that ginsenoside Rg3 (Rg3) increased cardiolipin depending on cardiolipin synthase 1 (CRLS1) in both worms and in human neural cells. Using LiP-SMap (limited proteolysis-mass spectrometry) strategy, we identified GRB2 (growth factor receptor bound protein 2) as a direct target of Rg3 in human neural cells. Rg3 enhances the binding between GRB2 and TRKA, that transduces signals *via* phosphrorylation of ERK. We provide bioinformatic and experimental evidence that EVI1, the critical oncogenic transcriptional regulator in leukemia, binds to *CRLS1* promoter region and stimulated *CRLS1* expression and subsequently increased cardiolipin content in the presence of Rg3. In a Parkinson's disease mouse model, Rg3 restores motor function by protecting nigral dopaminergic neurons dependent on Grb2. Our data recapitulate the TRKA-GRB2-EVI1-CRLS1 axis in maintaining proteostasis in Parkinson's disease *via* UPR^{mt}.

Keywords: Parkinson's disease; cardiolipin; UPR^{mt}; Ginsenoside Rg3; GRB2; TRKA; EVI1;

Introduction

Parkinson's disease (PD) is a neurodegenerative disease characterized by a progressive loss of dopaminergic neurons from the nigrostriatal pathway, formation of Lewy bodies, and microgliosis [1]. During the pathogenesis of PD, α-synuclein will misfold and aggregate in large quantities, forming amyloid oligomers, ribbons and fibers, which have been shown to cause neuronal toxicity by impairing numerous cellular processes [2]. Wealth of experimental data supports the hypothesis that the neurotoxicity of α-synuclein oligomers is intrinsically linked with their ability to interact with, and disrupt, biological membranes, especially those membranes having negatively-charged surfaces and/or lipid packing defects [3, 4].

Genetic data from familial and sporadic cases was used in an unbiased approach to build a molecular landscape for PD, revealing lipids as central players in this disease [5]. It is worth noting that compounds that cause fat accumulation can promote unfolded protein response (UPR) and help restore misfolded proteins [6]. Cardiolipin is a mitochondrial phospholipid involved in mitochondrial dynamics and functions [7]. Increasing the content of cardiolipin leads to stimulation of the mitochondrial UPR (UPR^{mt}), which helps to maintain proteostasis, protecting neuronal cells from the accumulation of unfoled and aggregates of toxic proteins, such as amyloid-β [8]. We sought to pharmacologically manipulate UPR^{mt} that restores cellular proteostasis to treat PD.

Rg3 improves Parkinson's symptoms based on lipid-increasing effect and unfolded protein response

It is worth noting that fat accumulation can promotes UPR and help cells remove misfolded proteins [6]. We therefore design a quaternary screening strategy to identify lipid modulating compounds that restores cellular proteostasis to treat PD. First, we used Nile Red to stain the lipid droplet of wild type *C.elegans* N2 strain [9]. From an in-house compound library composed of over 400 natural products [10], 18 lipid-increasing compounds were found (fig. S1A-B) in the primary screening. In the BZ555 strain (*dat-1*p::GFP), GFP is expressed specifically in dopaminergic (DA) neurons

under the control of dopamine transporter gene (*dat-1*) core promoter [9]. Upon 6-Hydroxydopamine (6-OHDA) treatment, DA neurons (GFP positive cells) die gradually, leading to the decrease of both GFP signal and GFP positive cell number. Using this assay, 6 compounds were found to protect DA neurons (fig. S1C-D) in the secondary screening. It has been reported that cardiolipin is necessary for the mitochondrial-to-cytosolic stress response (MCSR) induction and protects misfolded alpha-synuclein induced neural death [11]. We then check whether there are compounds that specifically increase cardiolipin content using 10-nonyl Acridine Orange (NAO) fluorescence dye [12]. We observed 3 compounds that increased NAO staining signals in the N2 strain (fig. S1E-F) in the tertiary screening. *Hsp-6* encodes a nuclear-encoded mitochondrion-specific chaperone related with the DnaK/HSP70 superfamily of molecular chaperones [6]. Using transgenic *C.elegans* SJ4100 strain (*hsp-6*p::GFP) [13], we could observe mitochondrial UPR (UPR^{mt}) directly by measuring GFP signals. In the quaternary screen, we found that only ginsenoside Rg3 upregulated *hsp-6* signals (fig. S1G-I).

Further, the screening results were verified using the transgenic *C.elegans* BZ555 strain. Rg3 decreased the loss of dopamine neurons in BZ555 strain dose dependengly (Fig. 1A, fig. S2A). To evaluated the efficacy of Rg3 in removing α-synuclein aggregates, we used the transgenic *C.elegans* NL5901 strain (*unc-54p*::α-synuclein::YFP) that overexpressed α-synuclein fused with YFP (yellow fluorescence protein) [9]. The content of α-synuclein was measured by YFP signals. It turned out that Rg3 treatment reduced the accumulation of α-synuclein in NL5901 strain in a dose dependent manner (Fig. 1B, fig. S2B). Rg3 treatment also increased cardiolipin content in N2 strain (Fig. 1C, fig. S2C). Meanwhile, Rg3 dose-dependently extended lifespan (mean = 23.9 days) to that of the solvent controls (mean = 17.3 days), comparable to L-DOPA (fig. S2D-E). These data suggest that Rg3 increases cardiolipin content to stimulate UPR^{mt} and is a potent anti-AD compound.

Cardiolipin is generated and metabolized by a series of enzymes (fig. S3A), to figure out which enzyme plays a key role in maintaining cardiolipin content in PD model, each of these enzymes was knocked down by RNAi. Only *crls1* RNAi led to

completely elimination of Rg3 efficacy in BZ555 worms (Fig. 1D). Consistent with previous data, suppressing *crls1* decreased cardiolipin content (fig. S3B-C). The *crls1* RNAi effect in PD model could be reversed by cardiolipin replenishment (Fig. 1E). 6-OHDA caused decrease of cardiolipin content (fig. S1E) and UPR^{mt} decrease (Fig. 1F), but did not affect ER UPR (UPR^{ER}) or heat shock response (HSR), as 6-OHDA did not affect GFP signals in worm strains representing UPR^{ER} (SJ4500, *hsp-4*p::GFP) and HSR (CL2070, *hsp-16.2*p::GFP) [6], respectively (fig. S3D-E). Rg3 increased *crls1* expression (fig. S3F) might compensate the cardiolipin loss upon 6-OHDA treatment and restore UPR^{mt} (Fig. 1G). The anti-PD effect of Rg3 was abrogated by *hsp-6* RNAi (Fig. 1H). These results indicate that the anti-PD effect of Rg3 is dependent on UPR^{mt}. In addition, cardiolipin supplement failed to rescue 6-OHDA treated BZ555 worms in presence of Rg3 after diminishing UPR^{mt} using *hsp-6* RNAi (Fig. 1I). Taken together, these results indicate that crls1 works upstream of UPR^{mt} in protecting 6-OHDA-induced neuron loss.

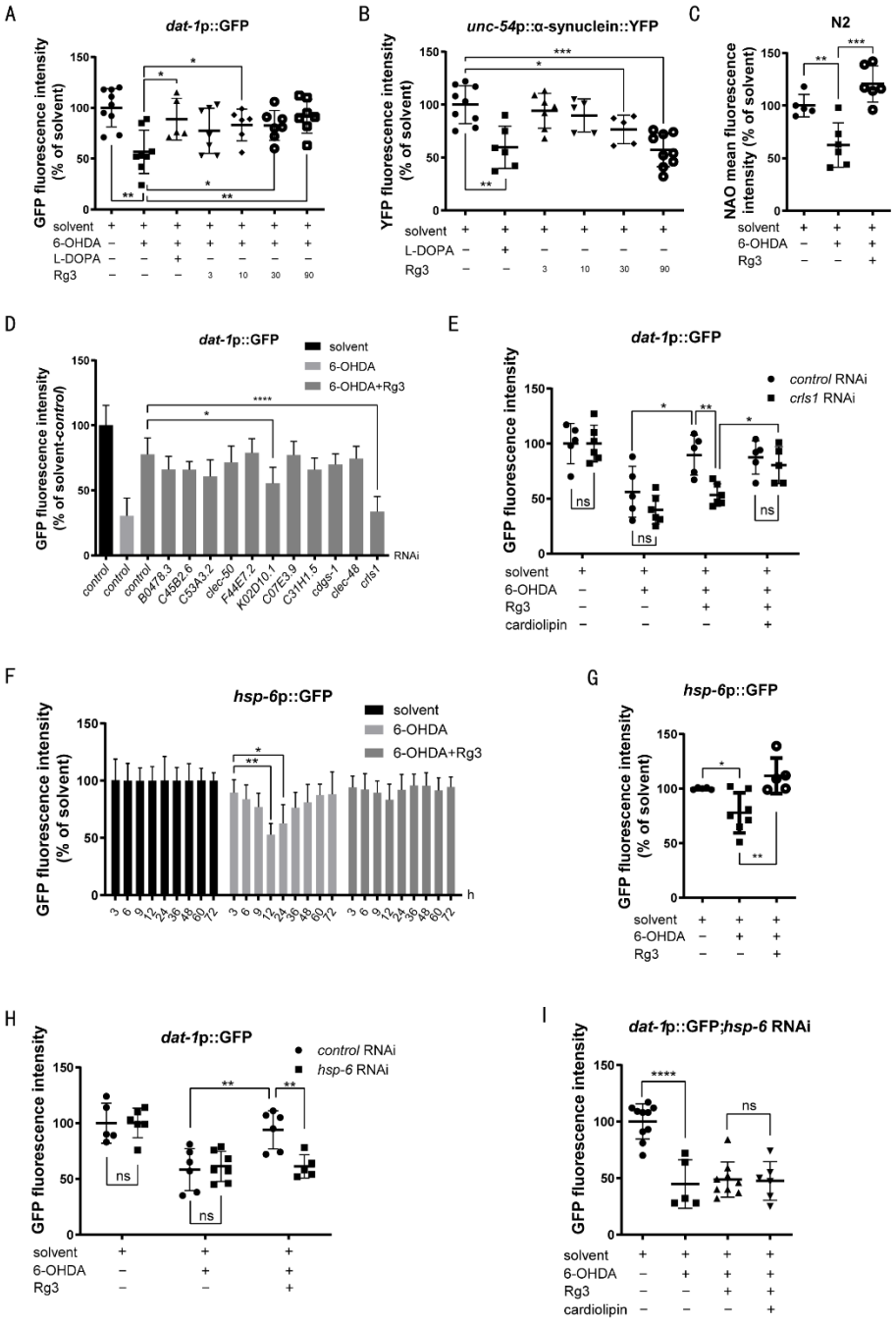

Figure 1. Rg3 improves Parkinson's symptoms based on lipid-increasing effect and unfolded protein response. (A) The BZ555 strain was pretreated with 6-OHDA (30 mM) for 1 h then transferred to the plates with 5-Fluorouridine (0.04 mg/mL) and indicated concentrations of Rg3 or L-DOPA (10 μM) for 72 h. The fluorescence intensity of dopaminergic neurons was measured. **(B)** The eggs of NL5901 strain were treated with indicated concentrations of Rg3 or L-DOPA (10 μM). After growing to the L4 stage, the nematodes were treated with 5-Fluorouridine (0.04 mg/mL) for 12 days. The fluorescence intensity of α-synuclein protein in nematodes was measured. **(C)** The N2 strain was pretreated 6-OHDA (30 mM) for 1 h then transferred to the plates with Rg3 (90 μM) for 36h. The cardiolipin content was measured by NAO (10 μM) fluorescence signaling. **(D-E)** The BZ555 strain was cultured for three generations on culture plates with bacteria containing

the indicated RNAi in the presence of Rg3 (90 μM). **(D)** Then the fluorescence intensity of dopaminergic neurons was measured. **(E)** The BZ555 strain was pretreated with 6-OHDA (30 mM) for 1 h then transferred to the plates with Rg3 (90 μM), 5-Fluorouridine (0.04 mg/mL) and cardiolipin (100 μg/ml) as indicated for 72 h. **(F)** The SJ4100 strain was treated with 6-OHDA (30 mM), 5-Fluorouridine (0.04 mg/mL) and Rg3 (90 μM) as indicated for different durations. The fluorescence representing UPR^{mt} was measured. **(G)** The SJ4100 strain was treated with Rg3 (90 μM) and 6-OHDA (30 mM) as indicated for 12 h, the fluorescence representing UPR^{mt} was measured. **(H)** The BZ555 strain fed with *hsp-6* RNAi was pretreated with 6-OHDA (30 mM) for 1 h then transferred to the plates with 5-Fluorouridine (0.04 mg/mL) and Rg3 (90 μM) as indicated for 72 h. **(I)** The BZ555 strain fed with *hsp-6* RNAi was pretreated with 6-OHDA (30 mM) for 1 h then transferred to the plates with 5-Fluorouridine (0.04 mg/mL), Rg3 (90 μM) and cardiolipin (100 μg/ml) as indicated for 72 h. * $p < 0.05$, ** $p < 0.01$, ***$p < 0.001$ vs. indicated control (n=5-12).

Rg3 promotes GRB2 and TRKA binding and facilitates CRLS1 expression in SH-SY5Y cells

Next, we validated the effect of Rg3 in mammalian neural cells. Rg3 dose dependently increased cell viability after SH-SY5Y cells were exposed to 6-OHDA (Fig. 2A). HEK293 cells overexpressing GFP-tagged α-synuclein were treated with Rg3, the accumulation of α-synuclein could be easily observed by GFP fluorescence signals. Rg3 clearly reduced α-synuclein-GFP signals, comparable to L-DOPA (fig. S4A). Consistent to *C.elegans* results, Rg3 restored 6-OHDA reduced cardiolipin content in neural cells, as shown by NAO staining (fig. S4B). In mammalian cells, the induction of UPR^{mt} resulted in upregulation of mitochondrial chaperone HSP70 (heat shock protein 70) [14]. The declined HSP70 level by 6-OHDA treatment was recovered by Rg3 dose dependently (fig. S4C), indicative of increased UPR^{mt}. The above data highlight the cross-species conservation of Rg3 efficacy in protecting neurons from 6-OHDA damages and α-synuclein proteotoxicity.

We then employed limited proteolysis-small molecule mapping strategy (LiP-SMap) to identify the direct target that interacts with Rg3 in proteomes [15]. We got 253 candidate proteins by LiP-SMap analysis (fig. S5A, table. S1). Ingenuity pathway analysis revealed the functional clusters of these 253 proteins (fig. S5B). According to the analysis and the literature study, we reduced the number of candidates to 10 proteins associated with Protein Ubiquitination Pathway and EIF2 Signaling, including USP9X,

GRB2, USP24, POGZ, RPL13, UBE4B, ELP2, DNAJC11, PSMD2 and TARDBP. SH-SY5Y cells were transfected with siRNA silencing these candidate genes (fig. S5C, table. S2-4) and then subjected to 6-OHDA and Rg3 treatment. It turned out that only when *GRB2* was silenced, the protective effects of Rg3 against 6-OHDA induced neural damages were fully abrogated (Fig. 2B). Further, we found that Rg3 enhanced the thermal stability of GRB2 (Fig. 2C). In addition, we measured the direct binding of GRB2 protein and Rg3. The K_D values of Rg3 and GRB2 were quite consistent using different methods including bio-layer interferometry (BLI) (K_D=1.53 ±0.11 μM, K_{ON} =6.16 ±0.34*10^3 $M^{-1}S^{-1}$, K_{Off} = 9.43 ±0.43*10^{-3} S^{-1}) (Fig. 2D) and microscale thermophoresis technology (MST) (K_D = 2.823 ± 4.16 μM) (fig. S5D). *In silico* molecular docking showed that Rg3 binds to Arg-67, Arg-86 and Leu-120 of GRB2 SH2 domain (fig. S5E).

It has been reported that the signaling adapter, GRB2, binds directly to the neurotrophin receptor tyrosine kinase (NTRK1 or TRKA) [16] and is essential for EGFR (epidermal growth factor receptor) signaling [17]. Then we checked whether Rg3 protects SH-SY5Y cells in a TRKA-dependent or EGFR-dependent manner. When SH-SY5Y cells were incubated with 6-OHDA (60 μM) for 3 hours, there was no change in the interaction between GRB2 and TRKA. Rg3 treatment promotes the interaction of GRB2 and TRKA in a dose-dependent manner (Fig. 2E). *In silico* molecular docking showed that binding of Rg3 to GRB2 increases the number of binding sites from 9 to 11 in the optimal binding mode of GRB2 and TRKA. (fig. S5F, table. S5-6). In contrast, Rg3 has no effect on the interaction between GRB2 and EGFR (Fig. 2E). ERK (extracellular regulated protein kinases) plays an important role in lipid synthesis [18] and is a key downstream factor related to TRKA [19, 20] and GRB2 [21]. As was shown, Rg3 increased phosphorylation of ERK in time-dependent (Fig. 2F) and dose-dependent (Fig. 2G) manners in SH-SY5Y cells. An ERK-specific inhibitor SCH772984 eliminated the effects of Rg3 on CRLS1 (Fig. 2H) and cardiolipin content (fig. S5G) [22]. However, GW441756, a specific TRKA inhibitor that binds to the extracellular domain of TRKA and blocks the binding of NGF (nerve growth factor) to TRKA (fig. S5H) [23], did not affect the Rg3 effects of activating ERK, increasing

CRLS1 and cardiolipin content (Fig. 2I, fig. S5G). Rg3 promoted a higher-molecular-mass species (MW: 250-300 kDa) containing GRB2 (MW: 25 kDa) in Native-PAGE that corresponded to the estimated combined masses of TRKA (MW: 130 kDa) dimer and GRB2, which was not abolished by GW441756 (Fig. S5I). Consistently, Rg3 increased phosphorylation of TRKA, which was also not abolished by GW441756 (Fig. S5J). Together, these results indicate that Rg3 glues GRB2 and TRKA together to activate TRKA downstream signaling and then up-regulate the expression of CRLS1. This effect is independent of NGF.

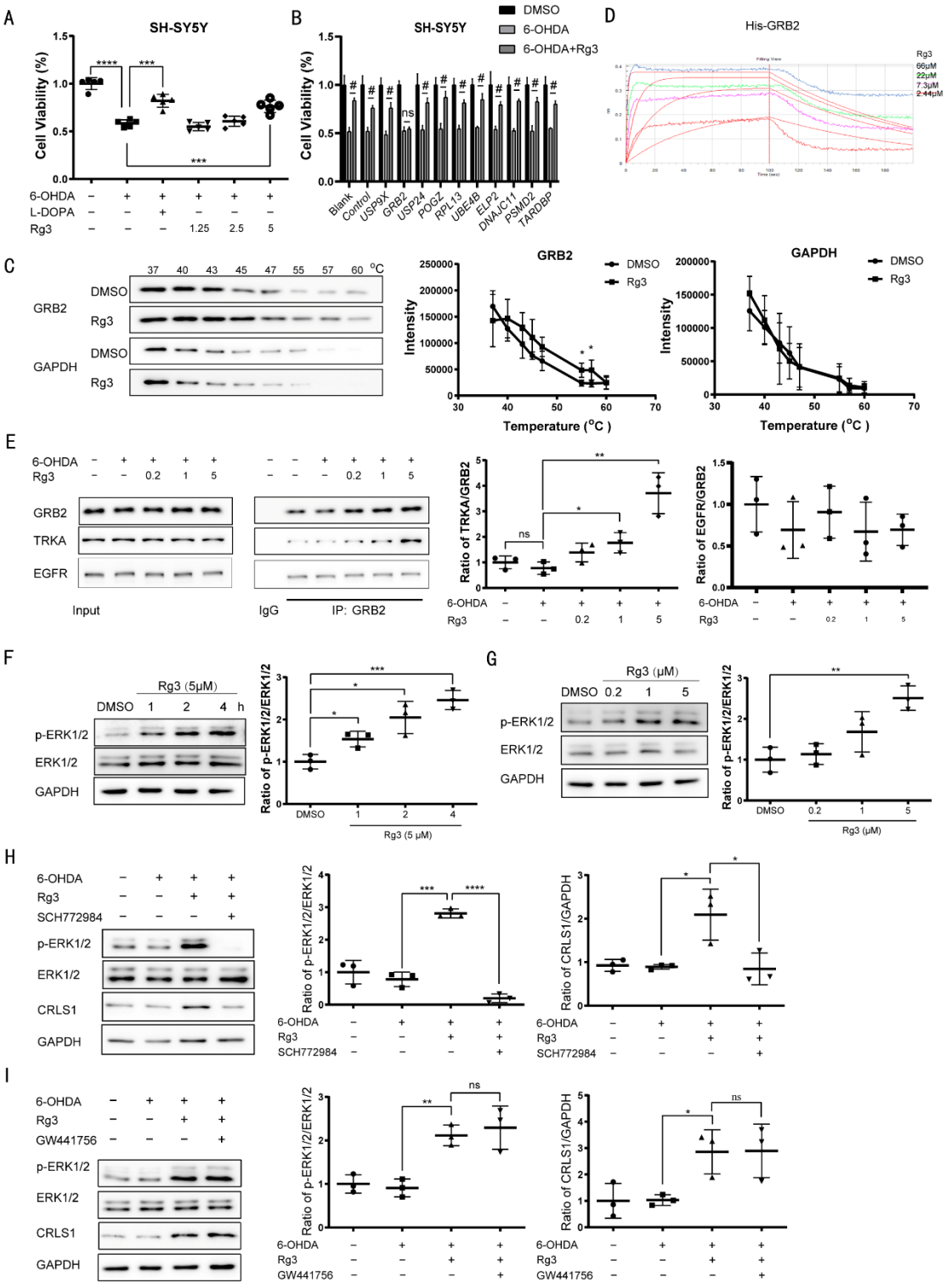

Figure 2. Rg3 promotes GRB2 and TRKA binding and facilitates cardiolipin synthase expression in SH-SY5Y cells. (A) SH-SY5Y cells were treated 6-OHDA (60μM) and indicated concentrations of Rg3 and L-DOPA (10 μM) for 24 h, then cell viability was measured by CCK8 assay. **(B)** SH-SY5Y cells were transfected with indicated siRNA for 6 h, then cultured with normal medium for 24h and treated with 6-OHDA (60μM) and Rg3 (5 μM) for additional 24 h. Cell viability was then measured by CCK8 assay. **(C)** SH-SY5Y cells were pretreated by DMSO or 5 μM Rg3 for 6 h. Then protein samples of each group

were collected and applied for thermal shift assay. **(D)** Four appropriate gradient concentrations of Rg3 (2.44, 7.3, 22, 66 μM) were selected, and the proper concentrations of the GRB2 proteins were all set at 1 mg/ml for the loading solution. The kinetic parameters, including K_{on}, K_{off} and K_D were calculated in a Fortebio Octet RED9696 instrument. **(E)** SH-SY5Y cells were treated with Rg3 (5 μM) and 6-OHDA (60μM) for 3 h. Total protein was extracted and subjected to IP study with indicated antibodies. **(F-I)** SH-SY5Y cells were treated with 6-OHDA (60μM) and Rg3 with various inhibitors, total protein lysates were collected and specific protein levels were detected by western blot. **(F)** SH-SY5Y cells were treated with 6-OHDA (60μM) and Rg3 (5 μM) for indicated periods of time. **(G)** SH-SY5Y cells were treated with Rg3 at indicated concentrations for 6 h. **(H)** SH-SY5Y cells were treated with 6-OHDA (60μM) and 0.1% DMSO, Rg3 (5 μM) or Rg3 (5 μM) + SCH772984 (10 μM) for 6 h. **(I)** SH-SY5Y cells were treated with 6-OHDA (60μM) and 0.1% DMSO, Rg3 (5 μM) or Rg3 (5 μM) + GW441756 (10 μM) for 3 h. All Experiments were repeated at least three times. *p < 0.05, **p < 0.01, ***p < 0.001, #p < 0.001 vs. indicated control.

Rg3 up-regulates *CRLS1* in an EVI1 dependent manner

To understand how *CRLS1* is transcriptionally regulated, we predicted the transcription factors (TFs) and related TFs binding sites using match tools from TRANSFAC. In the *CRLS1* promoter region, we found 4 putative TFs (table. S7). Each of these TFs was knocked down by siRNAs in SH-SY5Y cells (fig. S6A). Only *EVI1 (Ecotropic Virus Integration Site 1 Protein Homolog)* siRNA abrogated the neuroprotective effects of Rg3 in the presence of 6-OHDA (fig. S6B). *EVI1* encodes a critical oncogenic transcriptional regulator for hematopoietic stem cell proliferation [24]. The function of EVI1 in leukemia and solid tumors has been well investigated [25], while the role of EVI1 in the neural system remains unknown. We first checked the subcellular localization of EVI1 in SH-SY5Y cells by immunofluorescence staining. EVI1 was mainly localized in the nuclei (Fig. 3A). 6-OHDA treatment did not change the level of EVI1 in nuclei, while Rg3 had a significant effect of increasing nuclear EVI1, which was reversed by ERK inhibitor SCH772984 (Fig. 3A). Similar results were observed in the nuclear fraction of SH-SY5Y cells (Fig. 3B). These data suggest that EVI1 is downstream of ERK signaling. When *EVI1* was knocked down, Rg3 neither promoted *CRLS1* expression (Fig. 3C-D), nor increased cardiolipin levels (Fig. 3E) in SH-SY5Y cells.

Further, we validated the binding of EVI1 to *CRLS1* promoter region (Fig. 3F).

Electrophoretic mobility shift assays (EMSA) demonstrated that the 655/668 region (GGATAAAACTAGATT) was probably the EVI1 binding motif within the fragment of the *CRLS1* promoter (Fig. 3F-G, table S8). We further performed chromatin immunoprecipitation (ChIP) assays and found that EVI1 was recruited to the 609 to 845 bp region that contains a predicted EVI1 binding motif (Fig. 3H-I, table S9). In contrast, Rg3 did not affect other transcription factor HNF1A (Fig. 3J-K, table S9). Overall, these results indicate that EVI1 is a *bona fide* transcription factor of *CRLS1*. Rg3 increases the expression of *CRLS1 via* EVI1.

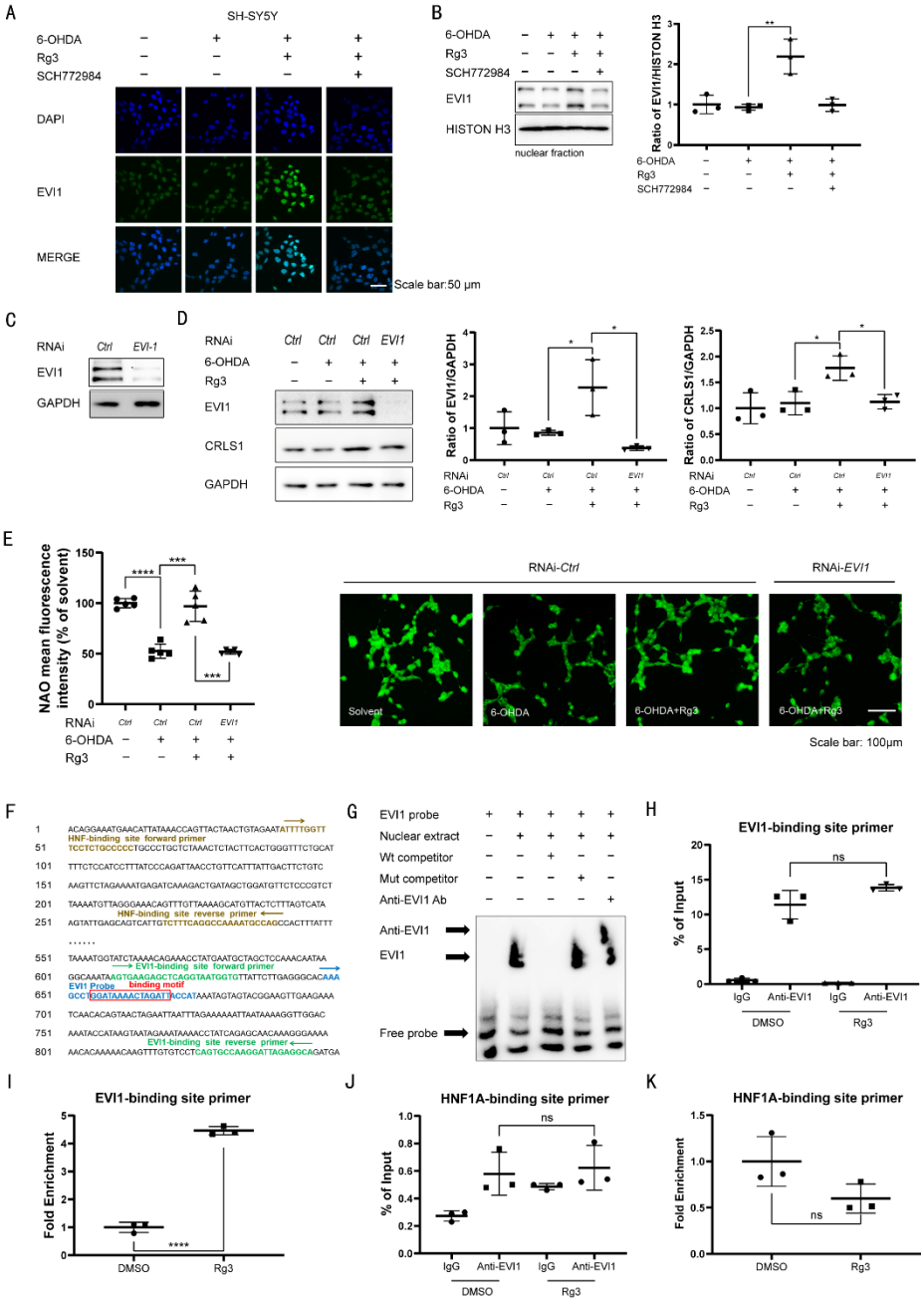

Figure 3. Rg3 up-regulates *CRLS1* in an EVI1 dependent manner. （A-B） SH-SY5Y cells were treated with 6-OHDA (60μM) and 0.1% DMSO, Rg3 (5 μM) or Rg3 (5 μM) + SCH772984 (10 μM) for 6 h. **(A)** Cells were fixed and immunostained with EVI-1 antibody. The representative images demonstrate the amount and localization of EVI-1 (green). Nuclei were counterstained with DAPI (blue). Scale bar: 50 μm. **(B)** Nucleoproteins were extracted and subjected to western blot with indicated antibodies. **(C-E)** SH-SY5Y cells were transfected with indicated siRNA for 6 h, then cultured with normal medium for 48h. Then Cells were treated with 6-OHDA (60μM) and Rg3 (5 μM) for 6 h. **(D)** Total proteins were extracted and subjected to western blot with indicated antibodies. **(E)** The cardiolipin content was measured by NAO (5 μM) fluorescence signaling. Scale bar: 100 μm. **(F)** A putative EVI1 probe binding site, a pair of EVI1 binding site primers and a pair of HNF1A binding site primers in the *CRLS1* promoter. **(G)** Electrophoretic mobility shift assay (EMSA) of EVI1 binding to the *CRLS1* promoter was performed with wildtype and mutant probes. Wt, wild type. Mut, mutant. Ab, antibody. **(H-I)** ChIP-qPCR analysis for the binding of EVI1 to the *CRLS1* promoter in SH-SY5Y cells treated with Rg3 (5 μM). **(J-K)** ChIP-qPCR analysis for the binding of HNF1A to the *CRLS1* promoter in SH-SY5Y cells treated with Rg3 (5 μM). All Experiments were repeated at least three times. *$p < 0.05$, **$p < 0.01$, ***$p < 0.001$, ****$p < 0.0001$ vs. indicated control.

Rg3 ameliorates MPTP-induced behavioral deficits through Grb2

Motor dysfunction is the main pathological character of PD patients and mouse models [26, 27]. MPTP produced reliable and reproducible damages to the nigrostriatal dopaminergic neurons [26]. To examine the protective effects of Rg3 in PD mouse model, we first measured motor function in the open field, accelerating rotarod, and pole tests on the day after the final Rg3 or normal saline (NS) administration in MPTP-treated mice (Fig. 4A). Total travelled distance during 3 minutes in mice treated with MPTP significantly reduced compared to control mice, which indicated the defect in autonomous activity. These impairments were reduced after Rg3 administration as the distance traveled by mice increased dramatically (Fig. 4B-C). In accord with pervasive motor dysfunction, MPTP-lesioned mice required more time to descend the pole and fell off the rotarod in less time than controls. Rg3 treatment reduced pole descent time (Fig. 4D). Further, Rg3 significantly increased rotarod time compared with the solvent group (Fig. 4E). Knockdown of *Grb2* in mouse neural cells (N2a) reversed Rg3 effects against 6-OHDA damages (fig. S7A-B), consistent to the results in human neural cells (Fig. 2B). AAV5 virus [28] carrying *Grb2* shRNA silenced *Grb2* in the substantial nigra (SN) of mice (fig. S7C, table. S3-4), which reversed the behavior benefits of Rg3 (Fig.

4B-E). Consistent to cell results, Rg3 increased Crls1 expression in the substantial nigra (SN) of mice (Fig. 4F). We next examined the neuroprotective efficacy of Rg3 by comparing nigral dopaminergic neuron numbers. MPTP-lesioned mice exhibited severe loss of tyrosine hydroxylase (Th)-protein and Th-positive neurons. Rg3 treatment greatly rescued Th level and Th-positive neurons (Fig. 4F-G). These findings suggested that the motor improvements (Fig. 4B-E) resulted from protection of nigrostriatal dopaminergic neurons. MPTP-lesioned mice exhibited enhanced Il-1β levels in the SN, which was reversed by Rg3 administration (Fig. 4G). The neuroprotection and anti-inflammation effects of Rg3 was completely abolished when *Grb2* in the SN was suppressed by AAV5-sh*Grb2* transduction. Together, these results suggest that Grb2 is essential for the therapeutic effects of Rg3 in protecting nigral dopaminergic neurons in mice.

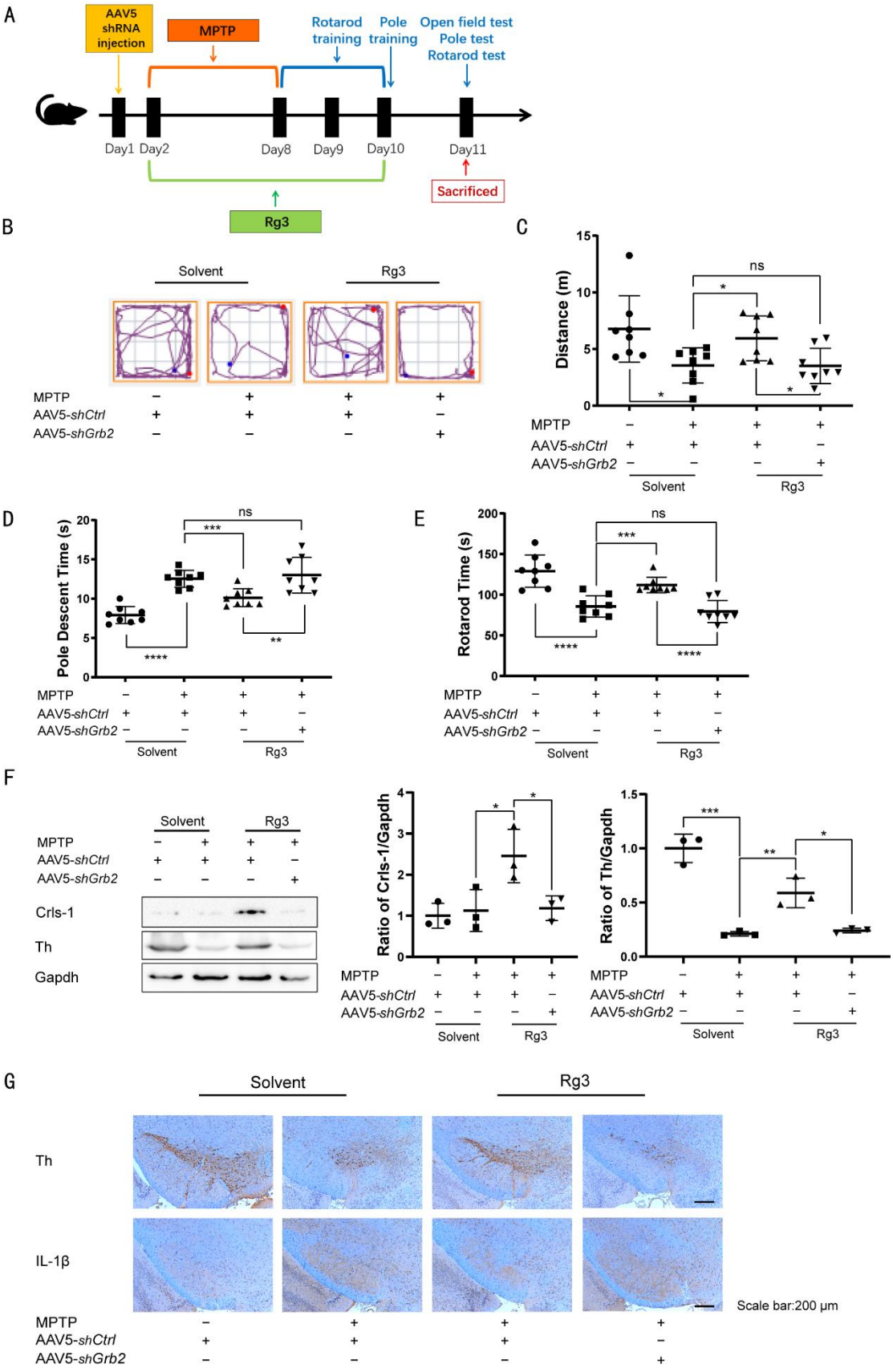

Figure 4. Rg3 ameliorates MPTP-induced behavioral deficits through Grb2. (A) The scheme of experimental procedure. A behavior-disordered PD model was induced by MPTP in C57BL/6J mice. Mice were then injected with AAV5-sh*GFP* (control group) or

AAV5-sh*Grb2* (*Grb2*-interfering group) in substantia nigra (n = 8 for each group). **(B-C)** Open field analysis of indicated mice. Total travelled distance in 3 minutes during test were recorded and analyzed. **(D)** Times required for mice to descend from the pole were recorded and analyzed. **(E)** Latency to fall during test on accelerated rotarod trials was recorded and analyzed. **(F)** Immunoblotting analysis of Th and Gapdh in the SN from 4 groups of mice as indicated. **(G)** Immunohistochemical staining for Th and Il-1β in the SN in these 4 groups of mice as indicated. *$p < 0.05$, **$p < 0.01$, ***$p < 0.001$, ****$p < 0.0001$ vs. indicated control.

Discussion

Brain tissue of PD patients and animal studies have shown that oxidative stress damages key cellular pathogenetic proteins that in turn cause these misfolded proteins to form small aggregates, facilitating PD development and multiple system atrophy [29, 30]. Maintaining proteostasis is critical to restore neural cell function and protect from cell death [31]. In the present study, we identified that Rg3 decreased the loss of dopamine neurons in BZ555 strain (Fig. 1A, fig. S1C-D) and promoted the cell viability in mammalian cells challenged by 6-OHDA or α-synuclein overexpression (Fig. 2A, fig. S4A). The function of Rg3 seems to be dependent on its role in enhancing cardiolipin content and UPR^{mt} that relies on a critical enzyme Crls1 controling cardiolin synthesis (Fig. 1E-I).

Ginsenoside Rg3, one of the major active components of ginseng, exhibits antitumor activity in various tumors [32] and neuroprotective effects with anti-oxidative stress and antiinflammation [33]. Although Rg3 has been shown to be neuroprotective by protecting N-Methyl-d-aspartate (NMDA)-induced neuronal death [34, 35] and inhibiting the opening of mitochondrial permeability transition pores to produce antioxidant effect in the brain [36], but the direct target proteins of Rg3 have not been identified so far. Using LiP-SMap methods, we were able to identify GRB2 as the potent Rg3 target protein in regulating cardiolipin homeostasis and relieving symptoms of PD. Of course, we select GRB2 among dozens of genes. The other genes might also interact with Rg3. However, these genes probably do not play major roles in the process of Rg3 induced neuroprotection (Fig. 2B). Mechanistically, we found that Rg3 promoted the binding of GRB2 and TRKA, thereby activating ERK

phosphorylation and stimulated transcription factor EVI1 nuclear localization and then activated *CRLS1* transcription (Fig. 3A-D).

NGF is highly expressed in the human substantia nigra (SN) and decreased dramatically during PD patients and animal models [37-40]. The use of NGF to treat neurodegerative disease is limited due to its constant occurred side effects including pain response and weight loss [41]. Rg3 helps to form TRKA-GRB2 complex that transduces signaling to activate ERK even independent of NGF (Fig. 2H-I). The function of Rg3 is quite unique than other molecular glue that normally aim to degrade target proteins [42, 43]. To our knowledge, this is the first molecular glue that activates a tyrosine kinase receptor. In addition, we discovered a novel EVI1-CRLS1 pathway that support neuroprotective effects of NGF/TRKA signaling pathway, besides cAMP response element-binding protein (CREB) [44-48]. This is a novel therapeutic strategy that maybe applicable to neurodegenerative disorders caused by proteopathies (Fig. S8).

References

1. Kalia, L.V. and A.E. Lang, *Parkinson's disease.* The Lancet, 2015. **386**(9996): p. 896-912.
2. Dias, V., E. Junn, and M.M. Mouradian, *The role of oxidative stress in Parkinson's disease.* J Parkinsons Dis, 2013. **3**(4): p. 461-91.
3. Ghio, S., et al., *Interaction of alpha-synuclein with biomembranes in Parkinson's disease--role of cardiolipin.* Prog Lipid Res, 2016. **61**: p. 73-82.
4. Perrin, R.J., et al., *Interaction of human alpha-Synuclein and Parkinson's disease variants with phospholipids. Structural analysis using site-directed mutagenesis.* J Biol Chem, 2000. **275**(44): p. 34393-8.
5. Xicoy, H., B. Wieringa, and G.J.M. Martens, *The Role of Lipids in Parkinson's Disease.* Cells, 2019. **8**(1).
6. Kim, H.E., et al., *Lipid Biosynthesis Coordinates a Mitochondrial-to-Cytosolic Stress Response.* Cell, 2016. **166**(6): p. 1539-1552 e16.
7. Paradies, G., et al., *Role of Cardiolipin in Mitochondrial Function and Dynamics in Health and Disease: Molecular and Pharmacological Aspects.* Cells, 2019. **8**(7).
8. Sorrentino, V., et al., *Enhancing mitochondrial proteostasis reduces amyloid-beta proteotoxicity.* Nature, 2017. **552**(7684): p. 187-193.
9. Malaiwong, N., et al., *Anti-Parkinson activity of bioactive substances extracted from Holothuria leucospilota.* Biomed Pharmacother, 2019. **109**: p. 1967-1977.
10. Wang, J., et al., *Triptolide Inhibits Amyloid-β Production and Protects Neural Cells by Inhibiting CXCR2 Activity.* Journal of Alzheimer's Disease, 2013. **33**: p. 217-229.
11. Ryan, T., et al., *Cardiolipin exposure on the outer mitochondrial membrane modulates alpha-synuclein.* Nat Commun, 2018. **9**(1): p. 817.
12. *Petit P, Glab N, Marie D, Kieffer H, Métézeau P. Discrimination of respiratory dysfunction in*

yeast mutants by confocal microscopy, image, and flow cytometry. Cytometry. 1996 Jan 1;23(1):28-38. doi: 10.1002/(SICI)1097-0320(19960101)23:1<28::AID-CYTO5>3.0.CO;2-I. PMID: 14650438.

13. Yoneda, T., et al., *Compartment-specific perturbation of protein handling activates genes encoding mitochondrial chaperones.* J Cell Sci, 2004. **117**(Pt 18): p. 4055-66.
14. Rolland, S.G., et al., *Compromised Mitochondrial Protein Import Acts as a Signal for UPR(mt).* Cell Rep, 2019. **28**(7): p. 1659-1669 e5.
15. Piazza, I., et al., *A Map of Protein-Metabolite Interactions Reveals Principles of Chemical Communication.* Cell, 2018. **172**(1-2): p. 358-372 e23.
16. MacDonald, J.I.S., et al., *Direct Binding of the Signaling Adapter Protein Grb2 to the Activation Loop Tyrosines on the Nerve Growth Factor Receptor Tyrosine Kinase, TrkA.* Journal of Biological Chemistry, 2000. **275**(24): p. 18225-18233.
17. Wang, Z. and M.F. Moran, *Requirement for the adapter protein GRB2 in EGF receptor endocytosis.* Science, 1996. **272**(5270): p. 1935-9.
18. Yang, A., et al., *MAPK/ERK and JNK pathways regulate lipid synthesis and cell growth of Chlamydomonas reinhardtii under osmotic stress, respectively.* Sci Rep, 2018. **8**(1): p. 13857.
19. Duchemin, A.M., et al., *GM1 ganglioside induces phosphorylation and activation of Trk and Erk in brain.* J Neurochem, 2002. **81**(4): p. 696-707.
20. Fukumoto, S., et al., *GD3 synthase gene expression in PC12 cells results in the continuous activation of TrkA and ERK1/2 and enhanced proliferation.* J Biol Chem, 2000. **275**(8): p. 5832-8.
21. Nishino, T., et al., *Behavioral analysis in mice deficient for GAREM2 (Grb2-associated regulator of Erk/MAPK subtype2) that is a subtype of highly expressing in the brain.* Mol Brain, 2019. **12**(1): p. 94.
22. Yan, Z., et al., *Inhibition of ERK1/2 in cancer-associated pancreatic stellate cells suppresses cancer-stromal interaction and metastasis.* J Exp Clin Cancer Res, 2019. **38**(1): p. 221.
23. Jung, E.J., S.Y. Lee, and C.W. Kim, *Proteomic analysis of novel targets associated with TrkA-mediated tyrosine phosphorylation signaling pathways in SK-N-MC neuroblastoma cells.* Proteomics, 2013. **13**(2): p. 355-67.
24. Yuasa, H., et al., *Oncogenic transcription factor Evi1 regulates hematopoietic stem cell proliferation through GATA-2 expression.* EMBO J, 2005. **24**(11): p. 1976-87.
25. Liang, B. and J. Wang, *EVI1 in Leukemia and Solid Tumors.* Cancers (Basel), 2020. **12**(9).
26. Jackson-Lewis, V. and S. Przedborski, *Protocol for the MPTP mouse model of Parkinson's disease.* Nat Protoc, 2007. **2**(1): p. 141-51.
27. Suresh, S.N., et al., *A novel autophagy modulator 6-Bio ameliorates SNCA/alpha-synuclein toxicity.* Autophagy, 2017. **13**(7): p. 1221-1234.
28. Cheng, J., et al., *Microglial autophagy defect causes parkinson disease-like symptoms by accelerating inflammasome activation in mice.* Autophagy, 2020: p. 1-13.
29. Roberts, R.F., R. Wade-Martins, and J. Alegre-Abarrategui, *Direct visualization of alpha-synuclein oligomers reveals previously undetected pathology in Parkinson's disease brain.* Brain, 2015. **138**(Pt 6): p. 1642-57.
30. Peelaerts, W., et al., *alpha-Synuclein strains cause distinct synucleinopathies after local and systemic administration.* Nature, 2015. **522**(7556): p. 340-4.
31. Sweeney, P., et al., *Protein misfolding in neurodegenerative diseases: implications and*

strategies. Transl Neurodegener, 2017. **6**: p. 6.

32. Tang, Y.C., et al., *Ginsenoside Rg3 targets cancer stem cells and tumor angiogenesis to inhibit colorectal cancer progression in vivo.* Int J Oncol, 2018. **52**(1): p. 127-138.
33. Hou, J., et al., *Ginsenoside Rg3 and Rh2 protect trimethyltin-induced neurotoxicity via prevention on neuronal apoptosis and neuroinflammation.* Phytother Res, 2018. **32**(12): p. 2531-2540.
34. Kim, S., et al., *Ginsenoside Rg3 antagonizes NMDA receptors through a glycine modulatory site in rat cultured hippocampal neurons.* Biochem Biophys Res Commun, 2004. **323**(2): p. 416-24.
35. Kim, J.H., et al., *Neuroprotective effects of ginsenoside Rg3 against homocysteine-induced excitotoxicity in rat hippocampus.* Brain Res, 2007. **1136**(1): p. 190-9.
36. Tian, J., et al., *20(S)-ginsenoside Rg3, a neuroprotective agent, inhibits mitochondrial permeability transition pores in rat brain.* Phytother Res, 2009. **23**(4): p. 486-91.
37. *Nerve growth factor levels in parkinson disease and experimental parkinsonian rats.*
38. *NGF in Experimental Models of Parkinson Disease.*
39. *Role of growth factors in degeneration and regeneration in the central nervous system; clinical experiences with NGF in Parkinson's and Alzheimer's disease.*
40. *Neurotrophic factors in Alzheimer's and Parkinson's disease brain.*
41. *Intracerebroventricular Infusion of Nerve Growth Factor in Three Patients with Alzheimer's Disease.*
42. Li, Z., et al., *Allele-selective lowering of mutant HTT protein by HTT-LC3 linker compounds.* Nature, 2019. **575**(7781): p. 203-209.
43. Isobe, Y., et al., *Manumycin polyketides act as molecular glues between UBR7 and P53.* Nat Chem Biol, 2020.
44. Arthur, J.S., et al., *Mitogen- and stress-activated protein kinase 1 mediates cAMP response element-binding protein phosphorylation and activation by neurotrophins.* J Neurosci, 2004. **24**(18): p. 4324-32.
45. *Cell Survival Promoted by the Ras-MAPK Signaling Pathway by Transcription-Dependent and -Independent Mechanisms.*
46. *Mediation by a CREB Family Transcription Factor of NGF-Dependent Survival of Sympathetic Neurons.*
47. *CREB: A Major Mediator of Neuronal Neurotrophin Responses.*
48. *An NGF-TrkA-Mediated Retrograde Signal to Transcription Factor CREB in sympathetic Neurons.*

ACKNKOWLEDGEMENTS

We thank Prof. Wenyuan Wang at the Interdisciplinary Research Center on Biology and Chemistry for help with Parkinson's disease model and human genetics.

Funding: This work was supported by the Ministry of Science and Technology of China (2019YFC1711000), National Natural Science Foundation of China (81973500), the Project Program of State Key Laboratory of Natural Medicines,

China Pharmaceutical University (SKLNMZZCX201820), the "Double First-Class" University Project (CPU2018GF04). **Author contributions:** X.X. conceived the project. L.-F.-R.Q., C.Q., S.L., and X.X. designed the experiments. L.-F.-R.Q., C.Q., S.L., C.P., M.Z., P.W., performed the experiments. L.-F.-R.Q., C.Q., S.L., C.P., M.Z., P.W., P.Y., P.L., and X.X. analyzed the data. L.-F.-R.Q., and X.X. wrote the paper with input from all authors. **Competing Interests:** The authors declare no competing financial interests.

Materials and methods

Reagents

Ginsenoside Rg3 was obtained from Chengdu Pufei De Biotech Co., Ltd (Sichuan, China), which was dissolved with 1% dimethylsulfoxide (DMSO) for the *in vitro* experiments, or with 0.5% carboxymethylcellulose sodium (CMC-Na) solution for the *in vivo* tests. 5-Fluorouridine, Acridine Orange 10-nonyl bromide (NAO), Nile Red, 1-Methyl-4-phenyl-1,2,3,6-tetrahydropyridine hydrochloride (MPTP), EZ-ChIP kit, KH_2PO_4, Na_2HPO_4, NaCl, iodoacetamide, protease K, DMSO, formic acid were purchased from Sigma-Aldrich (St. Louis, MO, USA). SCH772984 (HY-50846) and GW441756 (HY-18314) were purchased from MedChem Express (Shanghai, China). Tissue protein extraction kit, bicinchoninic acid (BCA) protein assay kit, EMSA/Gel-Shift kit, Coomassie blue G250 and DAPI (cat. No. AF0006) were obtained from Beyotime Institute of Biotechnology (Jiangsu, China). CMC-Na was purchased from Sangon Biotech Co., Ltd (Shanghai, China). AceQ qPCR SYBR Green Master Mix and HiScript QRT SuperMix for qPCR were purchased from Vazyme Biotech Co., Ltd. (Nanjing, China). Primary antibodies used in this study include Hsp70 Rabbit mAb (cat. No.AF1156, Beyotime, China), GAPDH Mouse mAb (cat. No. AF5009, Beyotime, China), TrkA Antibody (cat. No. 2505, Cell Signaling Technology, Beverly, USA), EGF Receptor Rabbit mAb (cat. No. 4267, Cell Signaling Technology, Beverly, USA), EVI-1 (C50E12) Rabbit mAb (cat. No. 2593, Cell Signaling Technology, Beverly, USA), Anti-rabbit IgG (H+L)-F(ab')2 Fragment-Alexa Fluor 555 Conjugate (cat. No. 4413, Cell Signaling Technology, Beverly, USA), CRLS1 pAb (cat. No. PA5-25338, Thermo, USA), GRB2 Rabbit mAb (cat. No. A19059, ABclonal, China), ERK1/ERK2 Rabbit pAb (cat. No. A16686, ABclonal, China), Phospho-ERK1-T202/Y204 + ERK2-T185/Y187 Rabbit pAb (cat. No. AP0472, ABclonal, China), Phospho-TrkA-Y490 Rabbit pAb (cat. No. AP0492, ABclonal, China), TH Rabbit pAb (cat. No. A0028, ABclonal, China), Histone H3 Rabbit pAb (cat. No. A2348, ABclonal, China), IL1 beta Rabbit pAb (cat. No. A16288, ABclonal, China). Secondary antibody was purchased from Beyotime

Institute of Biotechnology (Jiangsu, China). DMEM (cat. No. 11965-092) and FBS (cat. No.10100147) were from Gibco (USA). Penicillin and streptomycin, Trpsin and 4% paraformaldehyde were from KeyGEN (China). Mass spectrometry-grade trypsin was from Promega. Electrochemiluminescence (ECL) was from Tanon (China).

Worm Strains, culture, and synchronization

Wild-type: N2, NL5901 (pkIs2386 [*unc-54*p:: α-synuclein::YFP + unc-119(+)]), BZ555 (egIs1 [*dat-1*p::GFP]), SJ4100 (zcIs13[*hsp-6*p::GFP]), SJ4500 (zcIs4 [*hsp-4*p::GFP]V), CL2070 (dvIs[*hsp-16.2*p::GFP]) were obtained from the Caenorhabditis Genetics Center (University of Minnesota). Following the standard protocol, worms were fed by the lawn of *Escherichia coli* strain OP50. The worms were grown on solid nematode growth medium (NGM) plate in 20 °C incubator. The synchronized eggs were isolated by bleaching gravid adult worms in bleaching solution (12% NaClO and 10% 1M NaOH). Then, eggs were transferred into fresh NGM plate without OP50 and incubated overnight at 20 °C to obtain synchronized L1-stage worms. [1]

Inverted fluorescence microscope and image processing

Worms were immobilized with tetramisole and mounted on 6% agarose pads on glass slides. Images were acquired using inverted fluorescence microscope. For each condition, 5-7 fluorescence images of different worms were taken. Image processing was performed with Fiji software.

RNAi Treatment and RNAi Screening

RNAi treatment and RNAi screening were done according to a former research [2]. Briefly, synchronized eggs were harvested by bleaching and nematodes were grown on plates with *E. coli* OP50 until they reach early adulthood before transferred to RNAi plates. Day 1 adult worms are then grown on the RNAi plates with *E. coli* HT115 that carried the RNAi construct for 3 days at 20°C unless indicated otherwise in the figure legends. Worm eggs were synchronized by bleaching and grown on *E.*

coli OP50 plates until they reach day 1 adult at 25°C. Day 1 adult worms were transferred to *E. coli* HT115 RNAi plates and grown for 2 more days before the analysis.

Lipid deposition analyses

The nematode strain N2 worms [2] were washed off from plates with M9. Briefly, worms were fixed with freshly made 0.5% paraformaldehyde and frozen in liquid nitrogen immediately. M9 with Nile Red was added (1 μg/ml in final concentration) to the worms prior to staining for 15-30 min. Using a high-content screening instrument to take the fluorescence image of each well (TTP Labtech).

Nonyl Acridine Orange Staining

Nonyl Acridine Orange (NAO) was used to stain cardiolipin in nematode strain N2 [2]. After fixation and washing, 10 μM of NAO solution is added for 15-30 min, the fluorescence signaling represented cardiolipin content in worms.

Analysis of dopaminergic neurodegeneration and activation of UPR

Nematode strain BZ555 was used for analysis of dopaminergic neurodegeneration [1]. Nematode strain SJ4100, SJ4500 and CL2070 were used for analysis of UPR [2]. Synchronized L3 worms were treated with 30 mM 6-OHDA [3], 10 mM ascorbic acid, and diluted OP50 solution to induce DA neuron degeneration. Synchronized L3 worms were treated with 30 mM 6-OHDA (dissolved in 10 mM ascorbic acid) and diluted OP50 solution to induce DA neuron degeneration. Induced worms were then transferred onto NGM/OP50 plates containing indicated compound and 0.04 mg/ml 5-Fluorouridine. DMSO at final concentration of 1% (v/v) was applied in all treatments and used as a vehicle control. The fluorescence intensity of dopaminergic neurons was measured using inverted fluorescence microscopy (Nikon Ts2R).

Analysis of alpha synuclein protein aggregation

The α-synuclein expressing worms, NL5901 [1], were firstly synchronized. The newly hatched worms were transferred onto NGM/OP50 plates containing indicated compound and 0.04 mg/ml FUDR, incubated at 20 °C for 12 days.

Lifespan tests

Lifespan analyses were performed on synchronized L4 NL5901 [1] worms treated with indicated compound. The worms were counted and classified as alive, dead, or censored every day. The data were plotted as a survival curve and compared between groups.

Cell culture and Maintenance

SH-SY5Y cell, HEK293 and Neuro-2a (N2a) cell lines were obtained from the American Type Culture Collection. All of the cell lines were grown in DMEM (Gibco) containing 100 units/ ml penicillin and 100 μg/ml streptomycin sulfate (Keygen Biotechnology) with 10% FBS (Gibco) under 37°C, 5% CO2.

CCK8 assay

An *in vitro* Parkinson's disease (PD) model was established by treating SHSY5Y cells with 6-OHDA [4]. Cells were seeded in 96-well plate at a density of 1×10^4 cells *per* well for 24 h. After that, cells were treated with various concentrations of compounds. The proliferation of SH-SY5Y cells was evaluated by the cell counting kit-8 (CCK8) assay according to the manufacturer's instructions.

Transfection

HEK293 cells were transfected with human alpha-synuclein overexpressioin plasmid (Cat: HG12093-ANG, Sinobiological, Beijing, China) using Lipo3000. Human alpha-synuclein was tagged with N-terminal GFP. After incubating with plasmids for 6 hours, the supernatant was replaced by drug-containing solution or the control solution for 42 hours incubation. The amount of alpha-synuclein in cells was imaged by fluorescence microscopy (Nikon Ts2R).

Cell Cardiolipin Staining

SH-SY5Y cells were treated with blank solvent, 6-OHDA, and/or Rg3 for 24 hours. After 24 h of incubation, the supernatant was replaced by phenol red-free medium containing 5 μM NAO for 20 minutes on ice in the dark. NAO was washed out by phenol red-free medium 2-3 times. Fluorescence images were captured with an inverted fluorescence microscopy (Nikon Ts2R) and the average fluorescence intensity of each image was analyzed with Fiji software.

Limited proteolysis combined with mass spectrometry (LiP-SMap)

LiP-SMap was done according to a former report [5]. Briefly, proteomes were extracted and incubated with Rg3 or DMSO for 10 minutes at 25°C. Samples were subjected to limited proteolysis to generate structure-specific protein fragments. Fragments were then digested with the sequence-specific protease trypsin to generate peptide mixtures amenable to bottom-up proteomic analysis. The polypeptide samples were dissolved in 0.1% formic acid and detected by Orbitrap mass spectrometer (Thermo), with label-free quantitation (LFQ) analysis, search for differential proteins on MaxQuant platform *via* MS sensitivity.

Immunoprecipitation

Cells were harvested and suspended in lysis buffer (Cell Signaling Technology, 9806) containing protease and phosphatase inhibitors. The cell lysates were centrifuged for 10 min at 14,000 g at 4°C. About 10% of the supernatant was used for western blot as inputs, while the rest of homogenates were incubated with specific antibodies at 4°C overnight. Then add protein A/G sepharose beads (Thermo Fisher Scientific, 78609) for 2 h at 4°C. The immunoprecipitation beads were washed with cold PBS for five times, followed by western blotting analysis.

RNA interference

The siRNA oligos as listed in table S3 were synthesized by BIOSYNTECH (Suzhou, China). Cells were transfected with the siRNAs using Lipofectamine™ 3000

(Invitrogen) according to the manufacturer's manual and then harvested after 48 h. Control vector-transfected cells were used as controls for all the experiments.

Western blot

The protein samples from the brain tissues and cultured cells were harvested and suspended in lysis buffer (Beyotime Biotechnology, P0013J), and the protein contents were determined using the BCA method (Beyotime Biotechnology, P0009). The extracted proteins were separated by SDS-PAGE and then transferred to a nitrocellulose membrane. The membranes were blocked for 1 h at room temperature and then treated overnight at 4°C with the primary antibodies. After incubated with HRP conjugated secondary antibodies for 2 h at room temperature, immunoblots of the membranes were visualized by chemiluminescence detection kit (Tanon Science & Technology). To eliminate variations due to protein quantity and quality, the data was adjusted to GAPDH (glyceraldehyde-3-phosphate dehydrogenase).

Cells were lysed with Native-PAGE lysis buffer (50 mM Tris (pH 7.4), 150 mM NaCl, 1% NP-40, 0.25% sodium deoxycholat and protease inhibitor). The protein contents were determined using the BCA method (Beyotime Biotechnology, P0009). Lysates were mixed with Native-PAGE sample buffer 5X (Beyotime) and subjected to Native-PAGE using ExpressPlus™ 4-12% PAGE Gel (GenScript) and Tris-MOPS-SDS Running Buffer (GenScript). Then extracted proteins were transferred to a nitrocellulose membrane. The blocking and visualization steps are the same as above.

Real-time PCR

Total RNAs were isolated using Trizol reagents (Vazyme) according to the manufacturer's instructions. RNA concentrations were equalized and reverse transcribed into cDNA using HiScript Reverse Transcriptase kit (Vazyme). Gene expression level was measured by qRT-PCR using SYBR-green (Vazyme). Gene expression was normalized to GAPDH, primers used in this study was listed in table S4.

Immunofluorescence

Formaldehyde-fixed cells were incubated with indicated primary antibodies at 4 °C overnight, and then incubated with secondary antibodies for 1 h at room temperature. DAPI was added and incubated with cells for 5 min. Immunofluorescence was visualized and captured on a confocal microscope (Olympus FV3000).

***In Silico* molecular docking**

To analyze the binding affinities of small molecule compound to target protein and the possible binding sites, an *in silico* protein ligand docking software AutoDock 4.2 or Discovery Studio (BIOVIA) program was applied [6]. Briefly, Crystal structure file of target protein was downloaded from the RCSB protein data bank. Docked conformations were generated by Lamarckian genetic algorithm (LGA). After statistical analysis, the conformations with the lowest binding energies were performed to generate the interaction figures of ligands to target protein.

Binding of Rg3 to GRB2

The interaction of Rg3 and recombinant GRB2 was monitored by BLI using a Fortebio Octet RED96 instrument. In the gradient concentration binding experiment, four appropriate gradient concentrations of Rg3 (2.44, 7.3, 22, 66 μM) were selected, and the proper concentrations of the GRB2 proteins were all set at 1 mg/ml for the loading solution. The kinetic parameters, including K_{ON}, K_{Off} and K_D were calculated by data analysis. The interaction was further validated with Microscale Thermophoresis (MST) methods using Monolith NT.115 (Nanotemper). Rg3 titrated in different concentrations to purified recombinant human GRB2 protein. The reaction was performed in 50 mM Hepes, 50 mM NaCl, 0.01% Tween 20 and 2 mM $MgCl_2$. Then the samples were incubated in room temperature for 5 min before analyzing by microscale thermophoresis. In this instrument, an infra blue Laser (IB Laser) beam couples into the path of light (i.e. fluorescence excitation and emission) with a dichroic mirror and is focused into the sample fluid through the same optical element used for fluorescence imaging. The IB laser is absorbed by the aqueous

solution in the capillary and locally heats the sample with a 1/e 2 diameter of 25 μm. Up to 24 mW of laser power where used to heat the sample, without damaging the biomolecules. To analyze the thermophoresis of a sample, ten microliters were transferred in a glass capillary (NanoTemper, hydrophilic treated). Thermophoresis of the protein in presence of varying concentrations of compound was analyzed for 30 seconds. Measurements were performed at room temperature and standard deviation was calculated from three independent experiments.

Thermal shift assay

For the temperature-dependent thermal shift assay [7], 150 μL of lysates (3 mg/mL) from SHSY5Y cells were incubated with 5 μM of Rg3 at each temperature point from 43 to 60 °C for 3 min. Samples were repeatedly freezing and thawing by liquid nitrogen. Then, the samples were centrifuged at 20,000 g for 10 min at 4 °C to separate the supernatant and pellet. The supernatant was mixed with 5× loading buffer and then separated on a 10 % SDS-PAGE for immunoblotting analysis of GRB2.

Prediction of transcription factor

To investigate the regulation of genes, we predicted the transcription factors (TFs) regulating cardiolipin synthase 1. The promoter sequences (upstream 2000 bp) of genes were downloaded from UCSC (http://genome.ucsc.edu/). Then we predicted the TFs and related TF binding sites (TFBS) using match tool from TRANSFAC (http://gene-regulation.com/pub/databases.html), which provides data on eukaryotic transcription factors and their experimentally-proven binding sites (table S7).

Electrophoretic mobility shift assay (EMSA)

The probe set were designed and labeled with biotin to target the EVI1 binding sites on the CRLS1 promoter (table S8). Nuclear extracts from SH-SY5Y cells were incubated with biotin-labeled probes. A competition assay was conducted with either an unlabeled biotin probe containing a known EVI1 binding site (positive control) or

an unlabeled probe with mutated EVI1 binding site. A supershift assay was performed with an EVI1 antibody.

Chromatin immunoprecipitation (ChIP) and sequential ChIP assay

ChIP was performed with an EZ-ChIP kit as per the manufacturer's instructions (table S9, Primers used in ChIP assays). Briefly, cells with different treatments were lysed in lysis buffer and sonicated (15 s on and 90 s off, repeated 8 times). After precipitation with Agarose A for 30 min, the fragmented DNA was pulled down with EVI1 antibody and then subjected to amplification by qPCR. Afterwards, sequential ChIP assays were performed. Briefly, after elution from protein A Sepharose beads, the DNA-protein complex was subjected to a second immunoprecipitation with EVI1 antibody. Control cell or rabbit IgG was included. GAPDH in DNA prior to immunoprecipitation was amplified as a control.

Animals and experimental design

All experiments and animal care in this study were conducted in accordance with the National Institutes of Health guide for the care and use of Laboratory animals (NIH Publications No. 8023, revised 1978), and the Provision and General Recommendation of Chinese Experimental Animals Administration Legislation and approved by the Science and Technology Department of Jiangsu Province (SYXK (SU) 2016-0011). Male C57BL/6J mice (Yangzhou University, China) were housed on woodchip bedding in cages with 50–60% humidity and a 12 h light/dark cycle and given free access to food and water. In PD experiment, mice were randomly divided into 4 groups: control group, MPTP alone group, and two MPTP plus Rg3 treatment groups. The Grb2 knockdown fragment was ligated to an shRNA carrying AAV5 vector. The titers of adeno-associated virus (AAV) were between 1 × 10E13 and 2 × 10E13 vg/ml. Mice were anesthetized by intraperitoneal injection of 0.7% pentobarbital sodium and then fixed in a stereotaxic apparatus. A total of 2 × 10E9 units of scramble virus (control group, MPTP alone group, and one of MPTP plus Rg3 treatment groups) or virus targeting mouse Grb2 (another one of MPTP plus Rg3

treatment groups) in a 1 μl volume was slowly injected into the SN (AP: −3.3 mm; ML: ±1.3 mm; DV: −4.7 mm from bregma) at a rate of 0.2 μl/min using a 25 μl syringe. Control group mice were administered phosphate buffered saline (PBS) (vehicle) for 7 consecutive days by i.p. injection, while mice of the MPTP alone and MPTP plus baicalein groups were injected i.p. with 20 mg/kg MPTP (every 2 h for a total of four doses in 1 d) for 7 consecutive days to induce PD. Mice in the two MPTP plus Rg3 groups received intragastric Rg3 at 20 mg/kg/d 1 hour before MPTP treatment for 7 days and continued administration for an additional 2 days (total of 9 days), while Mice of the control group and MPTP alone group received intragastric 0.5% CMC-Na for 9 days in the same way. All mice were killed after behavioral testing conducted the day for immunohistochemistry and western blotting.

Open Field Test

Open field tests were conducted as described [8]. The apparatus was made of white plastic (50 × 50 cm). Mice were transferred to the experimental room 1 hour before testing for adaptation and then placed into the open field chamber for 3 minutes. The total distance travelled was recorded automatically during test.

Pole Test

Pole tests were conducted as described [8]. Briefly, a 0.5-m long pole was placed vertically into the home cage, and mice were placed at the top. The time required to descend back into the cage was recorded. On the day before the test, each mouse received 3 consecutive training trials, each separated by 30-minute rest periods. On the test day, 3 test trials were conducted with 3-minute intervals, and the average time to descend back into the cage was recorded.

Accelerating Rotarod Test

Accelerating rotarod tests were conducted as described [8]. Briefly, mice were placed on the accelerating rotarod, which accelerates from 0 to 40 rpm in 180 seconds and the latency to fall off was recorded. Mice were pretrained over 3 consecutive days at a

30-minute interval. On the test day, mice were evaluated on 3 trials conducted with 3-minute intervals.

Histological analysis

The fresh brain tissue was fixed with fixed liquid for more than 24 hours. Remove the tissue from the fixed liquid and trim the target tissue with a scalpel in the ventilation cupboard, and put the trimmed tissue and the label in the dehydration box. Dehydration and wax leaching: put the dehydration box into the dehydrator in order to dehydrate with gradient alcohol. 75% alcohol 4 hours, 85% alcohol 2 hours, 90% alcohol 2 hours, 95% alcohol 1 hour, anhydrous ethanol I 30 min, anhydrous ethanol II 30 min, alcohol benzene 5~10 min, xylene II 5~10 min, 65 °C melting paraffin I 1h, 65 °C melting paraffin II 1h, 65 °C melting paraffin III 1 hour. The wax-soaked tissue is embedded in the embedding machine. First, put the melted wax into the embedding frame, and before the wax solidifies, remove the tissue from the dewatering box and put it into the embedding frame according to the requirements of the embedding surface and affix the corresponding label. Cool at -20 °C freezing table, and after the wax is solidified, the wax block is removed from the embedded frame and repaired. Place the trimmed wax block on a paraffin slicer with a thickness of 4 μ m. The tissue is flattened when the slice floats on the 40 °C warm water of the spreading machine, and the tissue is picked up by the glass slides and baked in the oven at 60 °C. After the water-baked dried wax is melted, it is taken out and stored at room temperature. For immunofluorescent-based double labeling, the sequential staining procedure was followed. Brain sections were stained for Th and Il-1beta and images were acquired using a light microscopy (Ts2R, Nikon, Japan).

Statistical analysis

Results are shown as means ± standard deviation. Significant differences between the groups were evaluated using the Student's *t*-test. When three or more means are compared for statistical significance, one or two-way ANOVA was conducted with treatment or phenotype as the independent factors. When two groups of measurements

were examined for statistical significance, the two-sided Student's *t*-test was conducted. The survival curves of C. elegans lifespan were analyzed and compared using log-rank (Mantel-Cox) test.

1. Malaiwong, N., et al., *Anti-Parkinson activity of bioactive substances extracted from Holothuria leucospilota.* Biomed Pharmacother, 2019. **109**: p. 1967-1977.
2. Kim, H.E., et al., *Lipid Biosynthesis Coordinates a Mitochondrial-to-Cytosolic Stress Response.* Cell, 2016. **166**(6): p. 1539-1552 e16.
3. *<Neurotoxin-induced degeneration of dopamine neurons in Caenorhabditis elegans.pdf>*.
4. Xi, Y., et al., *MitoQ protects dopaminergic neurons in a 6-OHDA induced PD model by enhancing Mfn2-dependent mitochondrial fusion via activation of PGC-1alpha.* Biochim Biophys Acta Mol Basis Dis, 2018. **1864**(9 Pt B): p. 2859-2870.
5. Piazza, I., et al., *A Map of Protein-Metabolite Interactions Reveals Principles of Chemical Communication.* Cell, 2018. **172**(1-2): p. 358-372 e23.
6. Zheng, Z.G., et al., *Inhibition of HSP90beta Improves Lipid Disorders by Promoting Mature SREBPs Degradation via the Ubiquitin-proteasome System.* Theranostics, 2019. **9**(20): p. 5769-5783.
7. Jafari, R., et al., *The cellular thermal shift assay for evaluating drug target interactions in cells.* Nat Protoc, 2014. **9**(9): p. 2100-22.
8. Zhang, Q.S., et al., *Reassessment of subacute MPTP-treated mice as animal model of Parkinson's disease.* Acta Pharmacol Sin, 2017. **38**(10): p. 1317-1328.

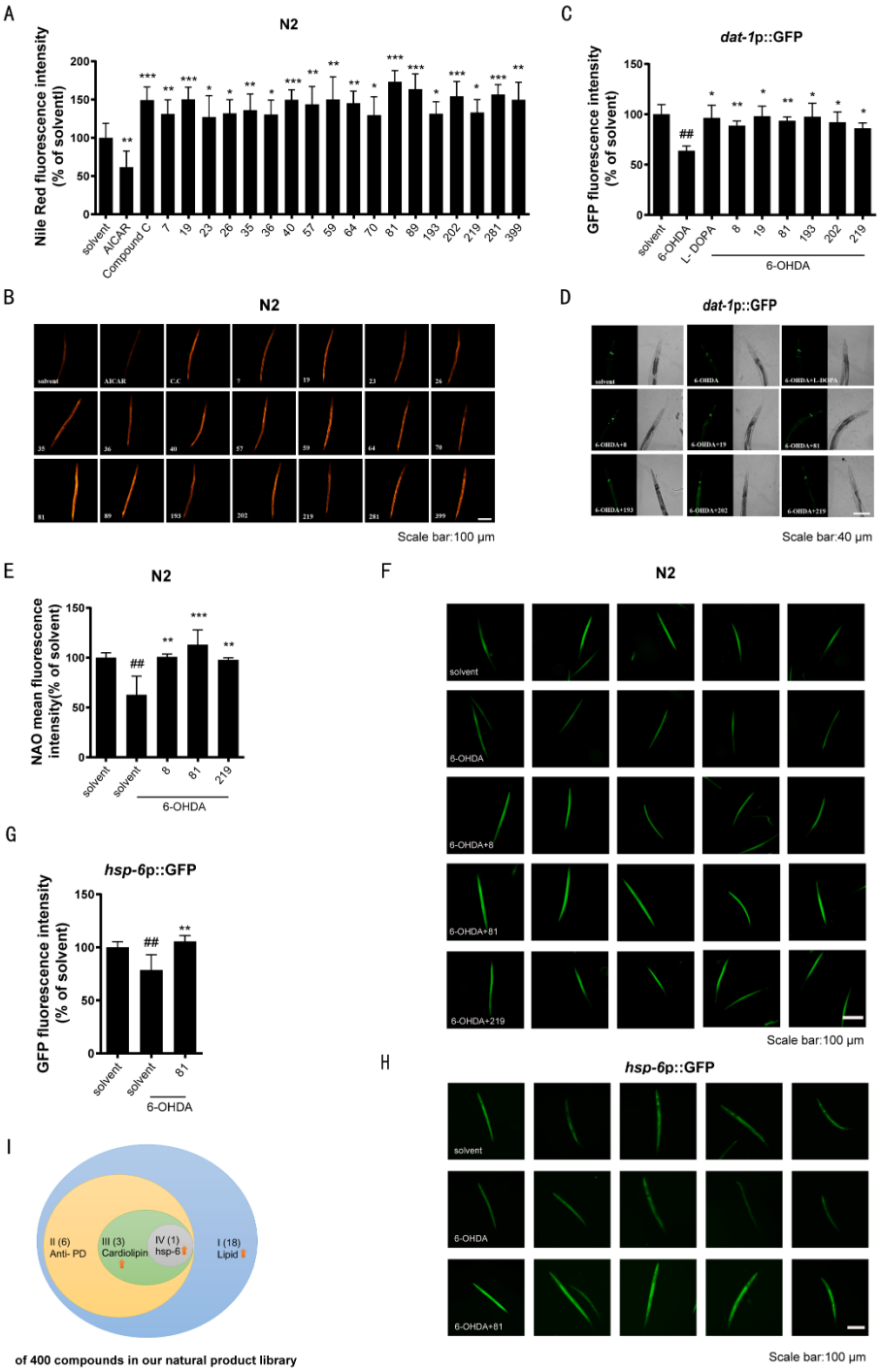

figure S1. (A-B) The N2 strain was treated with corresponding natural products (10 μM) or AICAR (1 mM) or Compound C (20 μM) for 24 h. The lipid droplet was measured with Nile Red (1 μg/ml) staining. Scale bar: 100 μm. **(C-D)** The BZ555 strain was pretreated with 6-OHDA (30 mM) for 1 h, and then transferred to plates containing indicated compound (10 μM) and 5-Fluorouridine (0.04 mg/ml) for 72 h. The fluorescence intensity of dopaminergic neurons was measured. Scale bar: 40 μm. **(E-F)** The N2 strain was pretreated with 6-OHDA (30 mM) for 1 h, then the nematodes were transfered to the plates containing indicated compound (10 μM) for 36h, followed by staining with NAO (10 μM). The fluorescence intensity of cardiolipin was measured. Scale bar: 100 μm. **(G-H)**

The SJ4100 strain was pretreated with 6-OHDA (30 mM) for 1 h, then the nematodes were transferred to the plates containing indicated compound (10 μM) for 12 h. The fluorescence intensity of nematodes was measured using inverted fluorescence microscopy. Scale bar: 100 μm. **(I)** Schematic diagram of screening results. ## $p < 0.01$ vs solvent-only control, *$p < 0.05$, **$p < 0.01$, ***$p < 0.001$ vs 6-OHDA control (n=5-8).

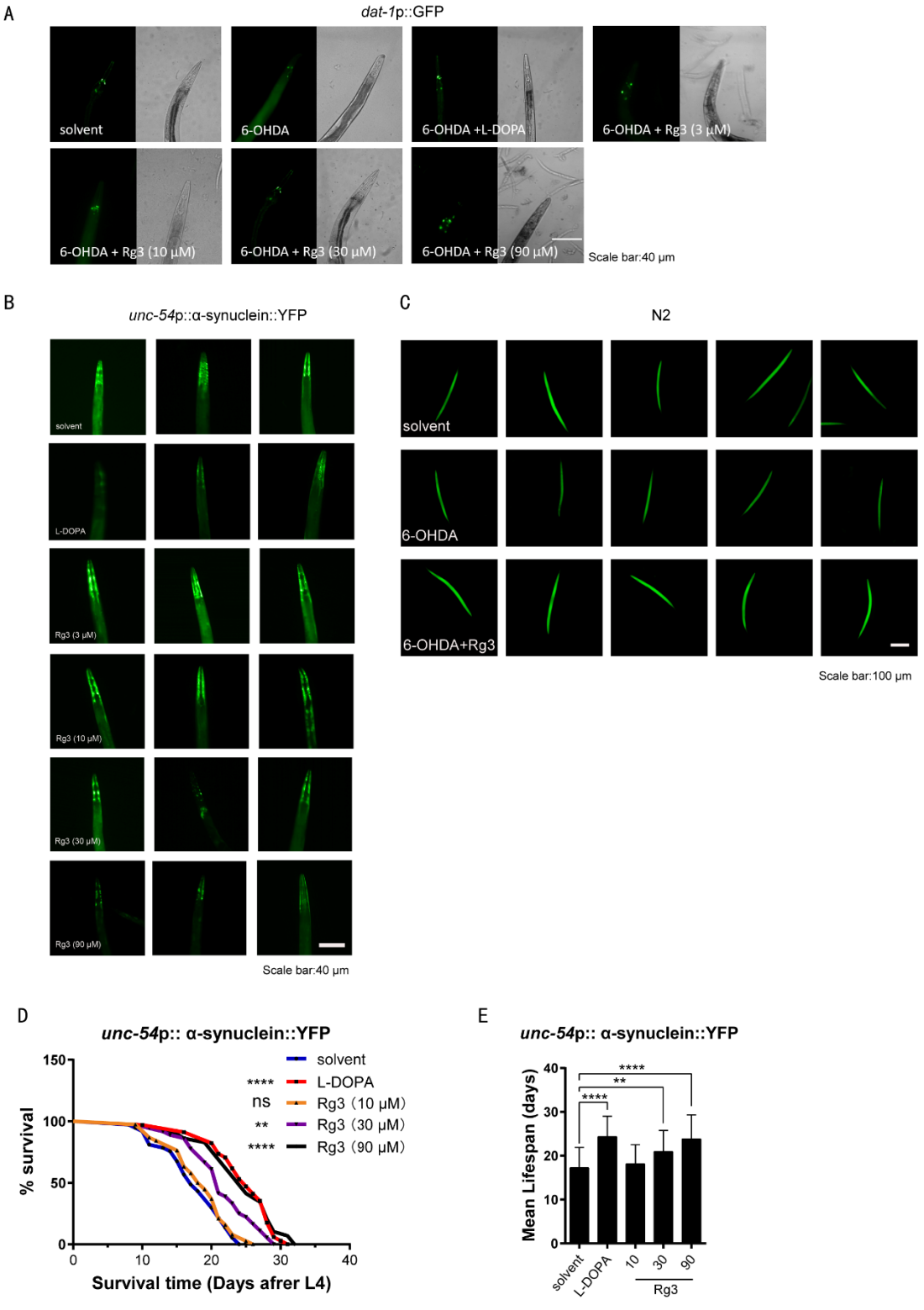

figure S2. (A) The BZ555 strain was pretreated with 6-OHDA (30 mM) for 1 h then transferred to the plates with 5-Fluorouridine (0.04 mg/mL) and indicated concentrations of Rg3 or L-DOPA (10 μM) for 72 h. The fluorescence intensity of dopaminergic neurons was measured. Scale bar: 40 μm. **(B)** The eggs of NL5901 strain were treated with indicated concentrations of Rg3 or L-DOPA (10 μM). After growing to the L4 stage, the nematodes were treated with 5-Fluorouridine (0.04 mg/mL) for 12 days. The fluorescence intensity of α-synuclein protein in nematodes was measured. Scale bar: 40 μm. **(C)** The N2 strain was pretreated 6-OHDA (30 mM) for 1 h then transferred to the plates with Rg3 (90 μM) for 36h. The cardiolipin content was measured by NAO (10 μM) fluorescence signaling. Scale bar: 100 μm. **(D-E)** The eggs of NL5901 strain were treated with indicated concentrations of Rg3 or L-DOPA (10 μM). After growing to the L4 stage, the nematodes were treated with 5-Fluorouridine (0.04 mg/mL). After 60 h, the number of nematodes was recorded every day. $^{**}p < 0.01$, $^{***}p < 0.001$, $^{****}p < 0.0001$ vs. indicated control (A-C: n=5-12; D-E: n=29-38).

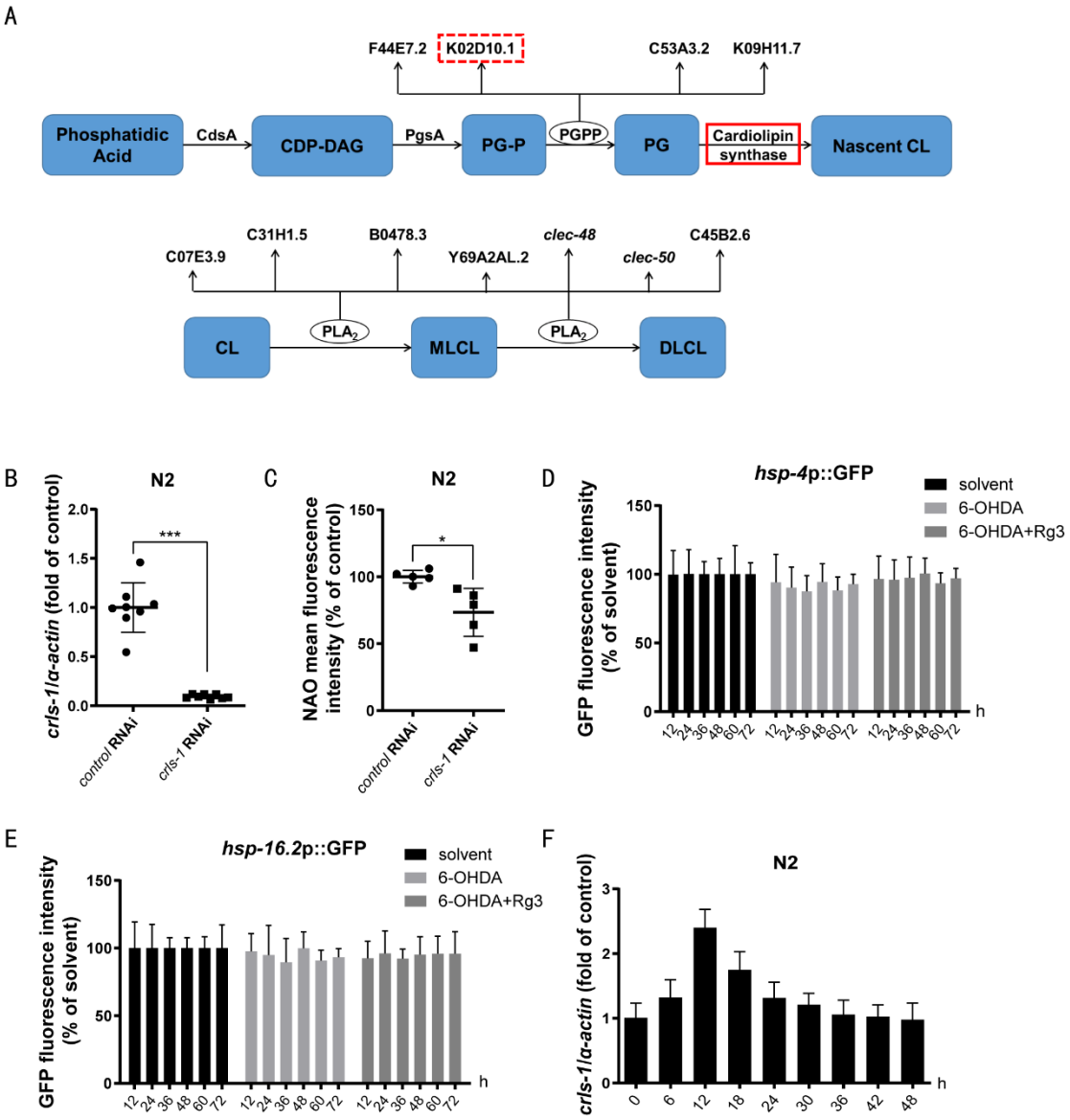

figure S3. (A) Genes involved in cardiolipin synthesis and hydrolysis. **(B)** The mRNA levels of *crls1* were measured in the N2 strain treated with *crls1* RNAi. **(C)** The *crls1* RNAi-treated N2 strain was stained with NAO (10 μM). Cardiolipin content was measured by the NAO fluorescence intensity. **(D-E)** The SJ4005 **(D)** and CL2070 strains **(E)** were treated with 6-OHDA (30 mM) for different durations. The green fluorescence signals representing UPR^{ER} and HSR were measured respectively. **(F)** The N2 strain was treated with Rg3 (90 μM) for different durations. The mRNA levels of *crls1* were measured by qRT-PCR. **p* < 0.05, ****p* < 0.001 vs. indicated control (n=4-8).

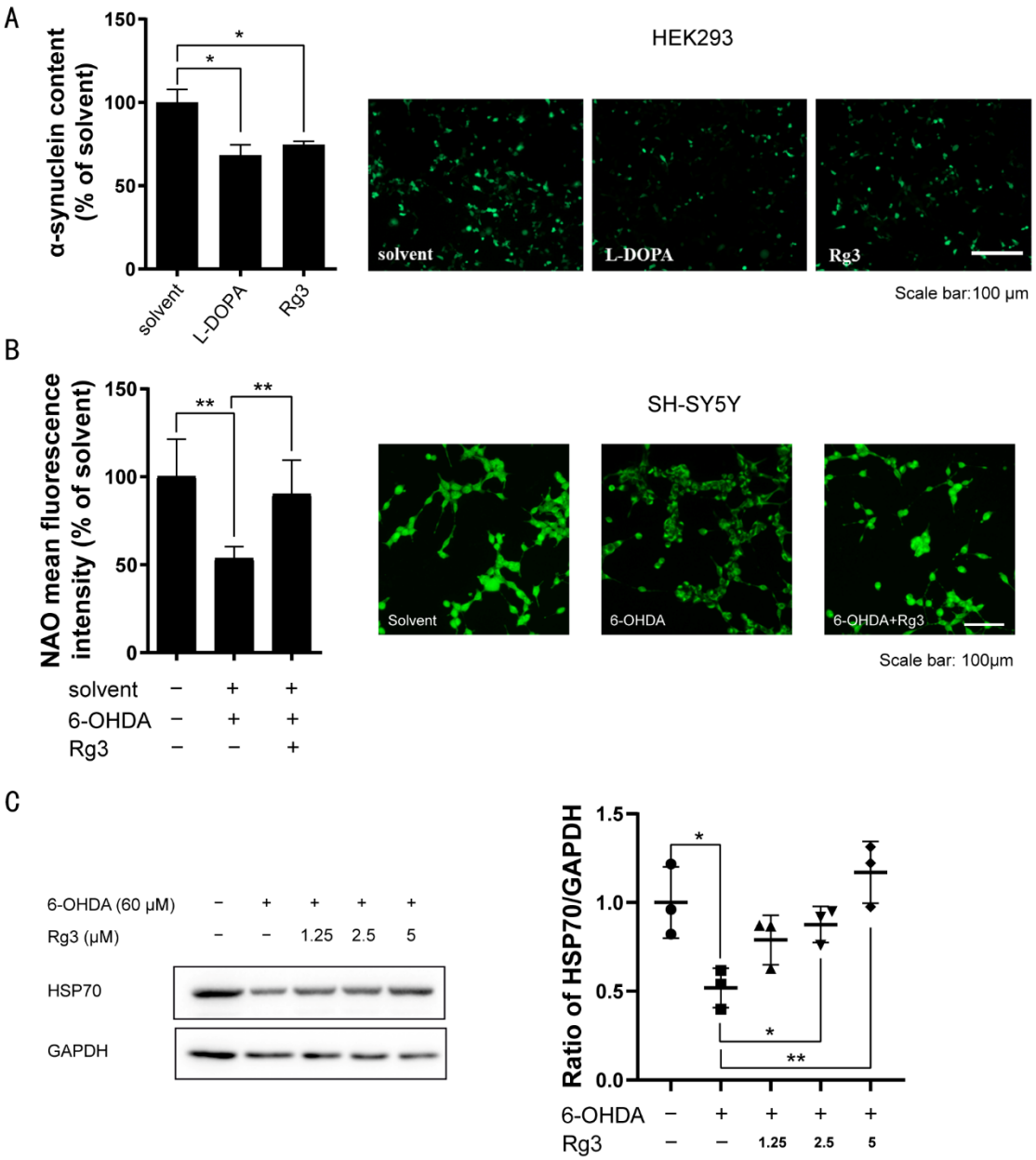

figure S4. (A) HEK293 cells were transfected with GFP-tagged α-synuclein plasmid, and then treated with Rg3 (5 μM) or L-DOPA (10 μM) for 48 h. The amount of α-synuclein protein level was measured by green fluorescence signals. Scale bar: 100 μm. **(B-C)** SH-SY5Y cells were treated with Rg3 (5 μM) and 6-OHDA (60 μM) for 24 h: **(B)** Fluorescence intensity of cells was measured by NAO (5 μM) fluorescence signaling. Scale bar: 100 μm. **(C)** Total proteins were extracted and subjected to western blot with indicated antibodies. All experiments were repeated at least three times, $*p < 0.05$, $**p < 0.01$ vs. indicated control.

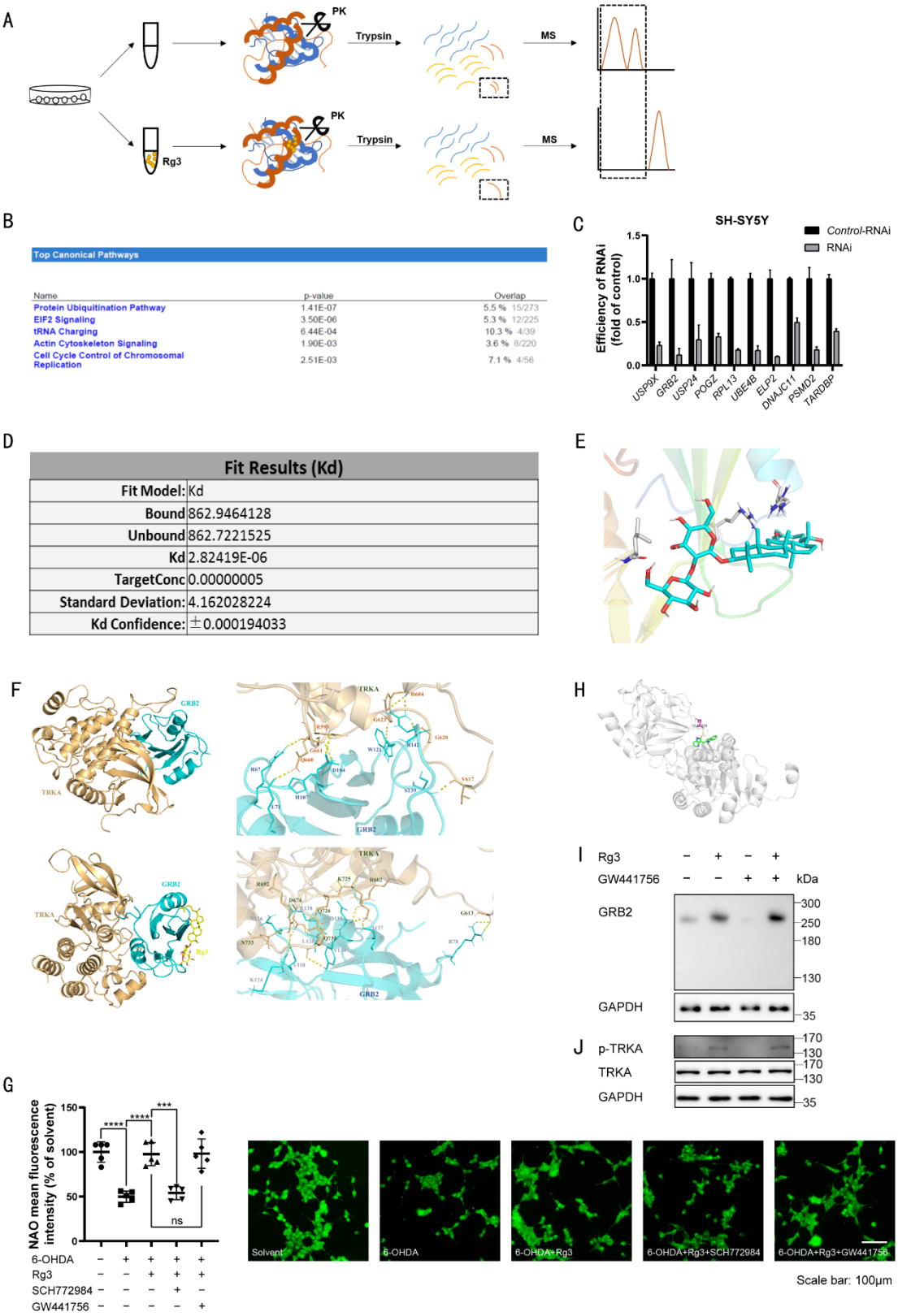

figure S5. (A) Diagram of LiP-SMap strategy. **(B)** Ingenuity pathway analysis of the 253 proteins. **(C)** SH-SY5Y cells were transfected with indicated siRNA for 6 h, then cultured with normal medium for 48h. The mRNA levels of indicated targets were measured by qRT-PCR. **(D)** Measurement of K_D value of the direct binding of GRB2 protein and Rg3 by Microscale Thermophoresis (MST). **(E-F)** *In silico* molecular docking using Discovery

Studio**. (E)** *In silico* molecular docking of the direct binding of Rg3 and GRB2 protein**. (F)** *In silico* molecular docking of the direct binding of TRKA and GRB2 protein (top). *In silico* molecular docking of the direct binding of TRKA and GRB2-Rg3 complex (below). **(G)** SH-SY5Y cells were treated with 6-OHDA (60 μM) and 0.1% DMSO, Rg3 (5 μM), Rg3 (5 μM) + SCH772984 (10 μM) or Rg3 (5 μM) + GW441756 (10 μM) as indicated for 24 h. The cardiolipin content was measured by NAO (5 μM) fluorescence signaling. Scale bar: 100 μm. **(H)** *In silico* molecular docking of the direct binding of TRKA protein and GW441756 (Autodock 4.2). **(I-J)** SH-SY5Y cells were treated with Rg3 (5 μM) and TRKA inhibitor GW441756 (10 μM) as indicated for 3 h. **(I)** Then protein samples of each group were collected and applied for Native-PAGE (GRB2) and WB (GAPDH) analysis. **(J)** Total proteins were extracted and subjected to western blot with indicated antibodies. ***p < 0.001, ****p < 0.0001 vs. indicated control.

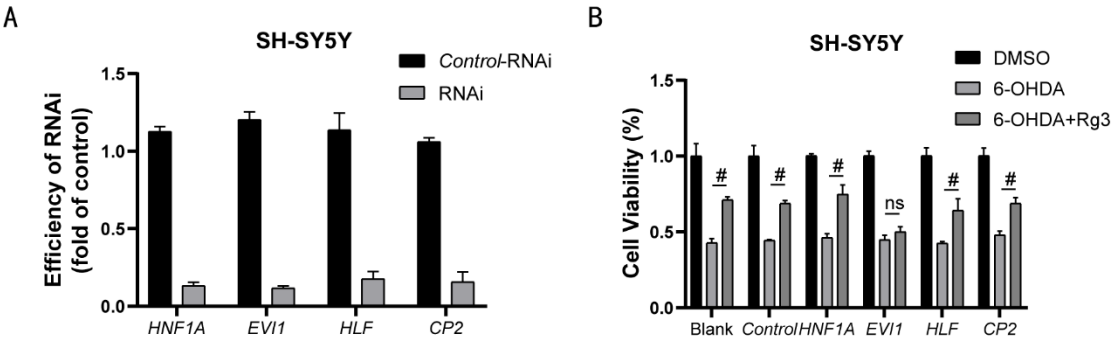

figure S6. (A) SH-SY5Y cells were transfected with indicated siRNAs for 6 h, then cultured with normal medium for 48h. The mRNA levels of indicated targets were measured. **(B)** After transfected with indicated siRNAs, cells were treated with Rg3 (5 μM) and 6-OHDA (60μM) as indicated for 24 h. Cell viability was measured by CCK8 assay. All experiments were repeated at least three times. #p < 0.0001 vs. indicated control.

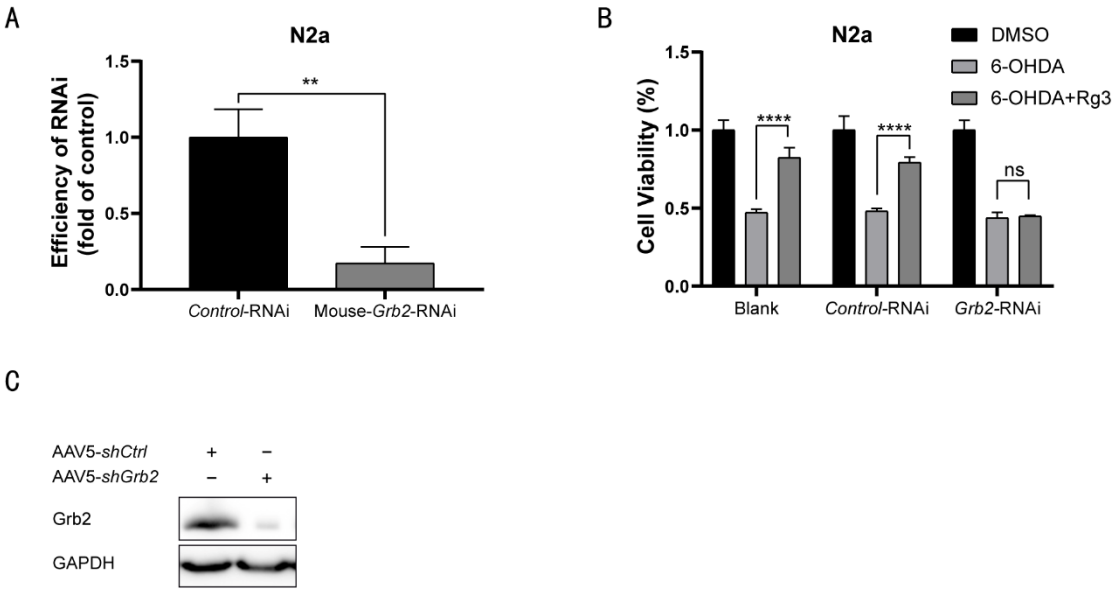

figure S7. (A) N2a cells were transfected with indicated siRNAs for 6 h, then cultured with normal medium for 48h. The mRNA levels of indicated targets were measured. **(B)** After transfected with indicated siRNAs, cells were treated with Rg3 (5 μM) and 6-OHDA (60μM) as indicated for 24 h. Cell viability was measured by CCK8 assay. **(C)** Immunoblotting analysis of Grb2 and Gapdh in the SN from 4 groups of mice as indicated. All experiments were repeated at least three times. **p < 0.01, ****p < 0.0001 vs. indicated control.

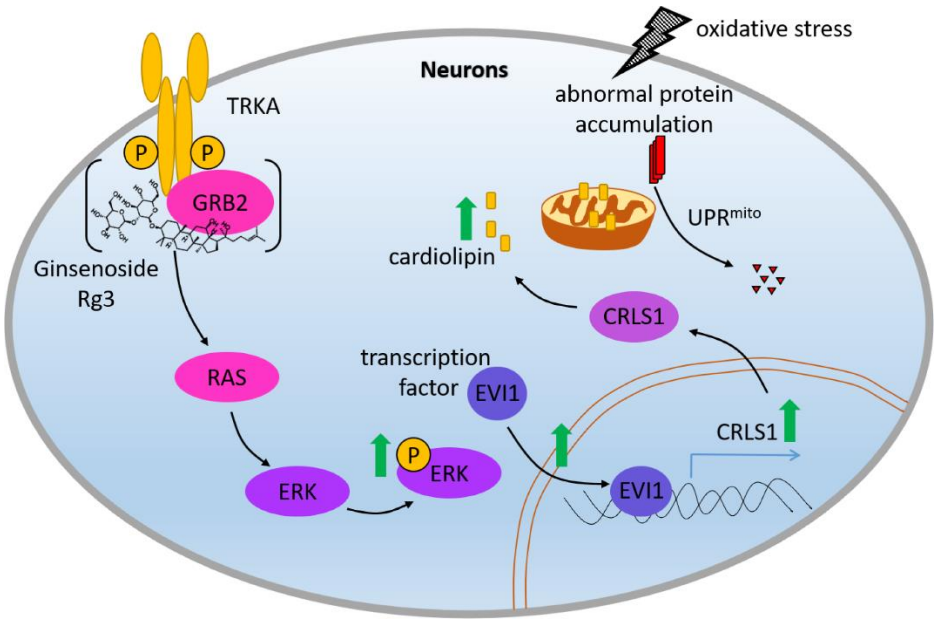

figure S8. Proposed mechanism of Rg3-mediated neuroprotective effects.

table S1. The result of LipSMAP

Proteins	Gene names	Protein names	aver(NC)	aver(Molecule)	ratio(M/NC)	P.Value
P26373	RPL13	60S ribosomal protein L13	4E+08	5E+06	0.013	0.009
P52272	HNRNPM	Heterogeneous nuclear ribonucleoprotein M	3E+08	5E+06	0.015	0.039
Q8NBT2	SPC24	Kinetochore protein Spc24	7E+07	5E+06	0.064	1E-05
P83916	CBX1	Chromobox protein homolog 1	2E+08	1E+07	0.078	5E-04
Q9NVG8	TBC1D13	TBC1 domain family member 13	1E+08	1E+07	0.078	0.003
Q7L1Q6	BZW1	Basic leucine zipper and W2 domain-containing protein 1	2E+08	2E+07	0.085	4E-06
Q9Y5P4	COL4A3BP	Collagen type IV alpha-3-binding protein	1E+07	1E+06	0.09	0.044
P07602	PSAP	Prosaposin;Saposin-A;Saposin-B-Val;Saposin-B;Saposin-C;Saposin-D	2E+08	3E+07	0.115	0.002
P01889	HLA-B	HLA class I histocompatibility antigen, B-7 alpha chain;	6E+08	7E+07	0.116	0.002
O15460	P4HA2	Prolyl 4-hydroxylase subunit alpha-2	1E+08	2E+07	0.145	0.008
P35580	MYH10	Myosin-10	3E+07	5E+06	0.156	0.016
Q9C0E2	XPO4	Exportin-4	1E+07	2E+06	0.167	0.027
Q9NVH1	DNAJC11	DnaJ homolog subfamily C member 11	2E+08	4E+07	0.172	2E-04
P49643	PRIM2	DNA primase large subunit	1E+08	2E+07	0.181	0.005
O00178	GTPBP1	GTP-binding protein 1	5E+07	9E+06	0.185	0.011
O75400	PRPF40A	Pre-mRNA-processing factor 40 homolog A	1E+08	2E+07	0.189	0.037
P05091	ALDH2	Aldehyde dehydrogenase	2E+08	4E+07	0.206	0.003
Q9H2M9	RAB3GAP2	Rab3 GTPase-activating protein non-catalytic subunit	1E+08	3E+07	0.207	0.038
Q9Y6D6	ARFGEF1	Brefeldin A-inhibited guanine nucleotide-exchange protein 1	2E+07	4E+06	0.219	0.004
Q9H4L5	OSBPL3	Oxysterol-binding protein-related protein 3	1E+07	3E+06	0.221	0.027
O95340	PAPSS2	Bifunctional 3-phosphoadenosine 5-phosphosulfate synthase 2;Sulfate adenylyltransferase;Adenylyl-sulfate kinase	5E+07	1E+07	0.221	0.002
Q6ZN17	LIN28B	Protein lin-28 homolog B	1E+07	3E+06	0.228	0.002
O60678	PRMT3	Protein arginine N-methyltransferase 3	5E+07	1E+07	0.228	0.03
Q6IA86	ELP2	Elongator complex protein 2	2E+07	4E+06	0.236	0.017
P08133	ANXA6	Annexin A6	3E+08	6E+07	0.241	0.008
Q96HS1	PGAM5	Serine/threonine-protein phosphatase PGAM5, mitochondrial	1E+08	3E+07	0.241	0.01
P62333	PSMC6	26S protease regulatory subunit 10B	1E+08	3E+07	0.245	0.003
P33176	KIF5B	Kinesin-1 heavy chain	8E+07	2E+07	0.257	0.045
P52294	KPNA1	Importin subunit alpha-5;Importin subunit alpha-5, N-terminally processed	5E+07	1E+07	0.263	0.028

Q13895	BYSL	Bystin	2E+07	5E+06	0.263	0.006
O14976	GAK	Cyclin-G-associated kinase	2E+07	6E+06	0.265	0.004
Q8WVV4	POF1B	Protein POF1B	1E+07	3E+06	0.27	0.012
Q93008	USP9X	Probable ubiquitin carboxyl-terminal hydrolase FAF-X	9E+06	3E+06	0.271	0.016
P49419	ALDH7A1	Alpha-aminoadipic semialdehyde dehydrogenase	4E+07	1E+07	0.276	0.024
P20020	ATP2B1	Plasma membrane calcium-transporting ATPase 1	1E+07	3E+06	0.292	0.042
P38606	ATP6V1A	V-type proton ATPase catalytic subunit A	2E+07	5E+06	0.292	0.037
Q9NVR2	INTS10	Integrator complex subunit 10	2E+07	6E+06	0.293	0.004
Q9NXE4	SMPD4	Sphingomyelin phosphodiesterase 4	2E+07	6E+06	0.293	0.045
Q9P287	BCCIP	BRCA2 and CDKN1A-interacting protein	1E+08	3E+07	0.298	0.044
Q5VT79	ANXA8L2	Annexin A8-like protein 2	4E+07	1E+07	0.299	0.008
P23381	WARS	Tryptophan--tRNA ligase, cytoplasmic;T1-TrpRS;T2-TrpRS	8E+07	2E+07	0.3	0.035
P38159	RBMX	RNA-binding motif protein, X chromosome;RNA-binding motif protein, X chromosome, N-terminally processed	5E+08	1E+08	0.301	0.046
P05023	ATP1A1	Sodium/potassium-transporting ATPase subunit alpha-1	6E+07	2E+07	0.303	0.003
P62917	RPL8	60S ribosomal protein L8	4E+07	1E+07	0.305	0.011
O43324	EEF1E1	Eukaryotic translation elongation factor 1 epsilon-1	9E+07	3E+07	0.313	0.038
P08708	RPS17	40S ribosomal protein S17	7E+07	2E+07	0.316	0.045
Q9BQ52	ELAC2	Zinc phosphodiesterase ELAC protein 2	6E+07	2E+07	0.321	0.024
Q8TBC4	UBA3	NEDD8-activating enzyme E1 catalytic subunit	2E+07	7E+06	0.325	0.009
P78527	PRKDC	DNA-dependent protein kinase catalytic subunit	3E+08	1E+08	0.326	0.005
O96019	ACTL6A	Actin-like protein 6A	1E+09	4E+08	0.326	0.013
Q14204	DYNC1H1	Cytoplasmic dynein 1 heavy chain 1	4E+07	1E+07	0.327	0.024
Q06830	PRDX1	Peroxiredoxin-1	3E+09	1E+09	0.328	0.026
P82912	MRPS11	28S ribosomal protein S11, mitochondrial	6E+07	2E+07	0.328	0.009
Q9UKK9	NUDT5	ADP-sugar pyrophosphatase	5E+07	2E+07	0.329	0.013
P53992	SEC24C	Protein transport protein Sec24C	2E+07	8E+06	0.332	0.003
Q6P2Q9	PRPF8	Pre-mRNA-processing-splicing factor 8	8E+07	3E+07	0.333	0.005
Q9UJ14	GGT7	Gamma-glutamyltransferase 7;Gamma-glutamyltransferase 7 heavy chain;Gamma-glutamyltransferase 7 light chain	1E+07	5E+06	0.338	0.015
Q9UPR3	SMG5	Protein SMG5	6E+07	2E+07	0.338	0.014
O94967	WDR47	WD repeat-containing protein 47	6E+08	2E+08	0.339	0.026
Q99543	DNAJC2	DnaJ homolog subfamily C member 2;DnaJ homolog subfamily C	3E+07	9E+06	0.339	0.004

		member 2, N-terminally processed				
Q06787	FMR1	Fragile X mental retardation protein 1	9E+07	3E+07	0.339	0.018
Q13523	PRPF4B	Serine/threonine-protein kinase PRP4 homolog	4E+07	1E+07	0.341	0.015
Q969X6	CIRH1A	Cirhin	4E+07	1E+07	0.343	0.003
Q96T76	MMS19	MMS19 nucleotide excision repair protein homolog	3E+07	9E+06	0.345	0.004
Q96AC1	FERMT2	Fermitin family homolog 2	5E+07	2E+07	0.345	0.014
Q92616	GCN1L1	Translational activator GCN1	6E+07	2E+07	0.345	0.048
Q9NRZ9	HELLS	Lymphoid-specific helicase	4E+07	1E+07	0.351	0.018
Q92890	UFD1L	Ubiquitin fusion degradation protein 1 homolog	8E+07	3E+07	0.353	0.015
P18206	VCL	Vinculin	7E+07	3E+07	0.353	0.016
P46939	UTRN	Utrophin	5E+08	2E+08	0.354	0.025
Q9NR09	BIRC6	Baculoviral IAP repeat-containing protein 6	1E+07	4E+06	0.354	0.023
Q9BV40	VAMP8	Vesicle-associated membrane protein 8	5E+07	2E+07	0.356	0.033
O43290	SART1	U4/U6.U5 tri-snRNP-associated protein 1	3E+07	1E+07	0.357	0.002
P22061	PCMT1	Protein-L-isoaspartate(D-aspartate) O-methyltransferase	5E+08	2E+08	0.358	0.027
P25685	DNAJB1	DnaJ homolog subfamily B member 1	5E+07	2E+07	0.361	0.001
P33176	KIF5B	Kinesin-1 heavy chain	1E+08	5E+07	0.362	0.043
Q9Y678	COPG1	Coatomer subunit gamma-1	6E+07	2E+07	0.362	0.029
Q8IWZ3	ANKHD1	Ankyrin repeat and KH domain-containing protein 1	2E+07	8E+06	0.363	0.012
Q13098	GPS1	COP9 signalosome complex subunit 1	5E+07	2E+07	0.364	0.005
Q92665	MRPS31	28S ribosomal protein S31, mitochondrial	6E+07	2E+07	0.366	0.016
Q969T9	WBP2	WW domain-binding protein 2	5E+07	2E+07	0.368	0.013
Q01518	CAP1	Adenylyl cyclase-associated protein 1	7E+07	3E+07	0.369	0.003
Q8NFH4	NUP37	Nucleoporin Nup37	9E+07	3E+07	0.369	0.016
Q99590	SCAF11	Protein SCAF11	2E+07	7E+06	0.369	0.004
Q15005	SPCS2	Signal peptidase complex subunit 2	7E+07	3E+07	0.373	0.033
P31431	SDC4	Syndecan-4	7E+07	3E+07	0.373	0.009
P48556	PSMD8	26S proteasome non-ATPase regulatory subunit 8	5E+08	2E+08	0.374	0.03
P02751	FN1	Fibronectin;Anastellin;Ugl-Y1;Ugl-Y2;Ugl-Y3	2E+07	6E+06	0.376	0.02
Q05682	CALD1	Caldesmon	5E+07	2E+07	0.376	0.006
P36405	ARL3	ADP-ribosylation factor-like protein 3	4E+07	1E+07	0.376	0.04
O95155	UBE4B	Ubiquitin conjugation factor E4 B	3E+07	1E+07	0.378	0.006
Q9NXG2	THUMPD1	THUMP domain-containing protein 1	4E+07	1E+07	0.383	0.008
Q9NR50	EIF2B3	Translation initiation factor eIF-2B subunit gamma	2E+07	7E+06	0.385	0.008
Q9UIQ6	LNPEP	Leucyl-cystinyl aminopeptidase;Leucyl-cystinyl	3E+07	1E+07	0.385	0.037

		aminopeptidase, pregnancy serum form				
P06737	PYGL	Glycogen phosphorylase, liver form	4E+07	1E+07	0.385	0.045
P27708	CAD	CAD protein;Glutamine-dependent carbamoyl-phosphate synthase;Aspartate carbamoyltransferase;Dihydroorotase	4E+07	1E+07	0.389	0.032
Q7LGA3	HS2ST1	Heparan sulfate 2-O-sulfotransferase 1	2E+07	9E+06	0.391	0.005
P18583	SON	Protein SON	3E+07	1E+07	0.392	0.012
Q9BRX2	PELO	Protein pelota homolog	7E+07	3E+07	0.395	0.009
Q7Z2T5	TRMT1L	TRMT1-like protein	2E+07	9E+06	0.396	0.006
Q9Y5Q8	GTF3C5	General transcription factor 3C polypeptide 5	3E+07	1E+07	0.396	0.017
P18124	RPL7	60S ribosomal protein L7	2E+08	9E+07	0.397	0.001
Q9Y4E8	USP15	Ubiquitin carboxyl-terminal hydrolase 15	4E+07	1E+07	0.397	0.031
Q9H583	HEATR1	HEAT repeat-containing protein 1;HEAT repeat-containing protein 1, N-terminally processed	2E+07	9E+06	0.398	0.008
Q14151	SAFB2	Scaffold attachment factor B2	1E+08	5E+07	0.398	0.022
P53992	SEC24C	Protein transport protein Sec24C	4E+07	2E+07	0.4	0.015
P54886	ALDH18A1	Delta-1-pyrroline-5-carboxylate synthase;Glutamate 5-kinase;Gamma-glutamyl phosphate reductase	2E+07	8E+06	0.4	0.005
O95817	BAG3	BAG family molecular chaperone regulator 3	7E+07	3E+07	0.402	0.006
Q8N766	EMC1	ER membrane protein complex subunit 1	4E+07	1E+07	0.402	0.011
O43432	EIF4G3	Eukaryotic translation initiation factor 4 gamma 3	2E+07	7E+06	0.403	0.008
Q8NBN7	RDH13	Retinol dehydrogenase 13	3E+07	1E+07	0.405	0.008
O75643	SNRNP200	U5 small nuclear ribonucleoprotein 200 kDa helicase	1E+08	5E+07	0.405	0.022
Q96P70	IPO9	Importin-9	5E+07	2E+07	0.411	0.009
Q9H2G2	SLK	STE20-like serine/threonine-protein kinase	8E+07	3E+07	0.412	0.002
O00468	AGRN	Agrin;Agrin N-terminal 110 kDa subunit;Agrin C-terminal 110 kDa subunit;Agrin C-terminal 90 kDa fragment;Agrin C-terminal 22 kDa fragment	2E+07	8E+06	0.413	0.018
Q96JB5	CDK5RAP3	CDK5 regulatory subunit-associated protein 3	5E+07	2E+07	0.416	0.002
O43809	NUDT21	Cleavage and polyadenylation specificity factor subunit 5	2E+08	1E+08	0.417	0.044
Q8N1G2	CMTR1	Cap-specific mRNA (nucleoside-2-O-)-methyltransferase 1	3E+07	1E+07	0.418	0.024
Q9UPU5	USP24	Ubiquitin carboxyl-terminal hydrolase 24	2E+07	7E+06	0.418	0.025
Q13148	TARDBP	TAR DNA-binding protein 43	4E+07	2E+07	0.419	0.045

O00483	NDUFA4	Cytochrome c oxidase subunit NDUFA4	9E+07	4E+07	0.42	0.04
Q96KB5	PBK	Lymphokine-activated killer T-cell-originated protein kinase	9E+07	4E+07	0.42	0.021
O14744	PRMT5	Protein arginine N-methyltransferase 5;Protein arginine N-methyltransferase 5, N-terminally processed	1E+08	5E+07	0.421	4E-05
Q6PI48	DARS2	Aspartate--tRNA ligase, mitochondrial	1E+08	4E+07	0.422	0.024
Q9BS26	ERP44	Endoplasmic reticulum resident protein 44	4E+07	2E+07	0.422	0.024
P41091	EIF2S3	Eukaryotic translation initiation factor 2 subunit 3	1E+08	5E+07	0.425	0.015
Q9UBU9	NXF1	Nuclear RNA export factor 1	2E+07	9E+06	0.425	0.01
Q8NI36	WDR36	WD repeat-containing protein 36	2E+07	8E+06	0.425	0.022
Q6DKJ4	NXN	Nucleoredoxin	4E+07	2E+07	0.426	0.03
Q9NTJ3	SMC4	Structural maintenance of chromosomes protein 4	7E+07	3E+07	0.427	0.005
Q86XL3	ANKLE2	Ankyrin repeat and LEM domain-containing protein 2	1E+07	4E+06	0.428	0.045
Q00341	HDLBP	Vigilin	6E+07	3E+07	0.429	0.047
Q96S59	RANBP9	Ran-binding protein 9	3E+07	1E+07	0.429	0.002
Q3LXA3	DAK	Bifunctional ATP-dependent dihydroxyacetone kinase/FAD-AMP lyase (cyclizing);ATP-dependent dihydroxyacetone kinase;FAD-AMP lyase (cyclizing)	2E+07	1E+07	0.429	0.022
Q9BRT9	GINS4	DNA replication complex GINS protein SLD5;DNA replication complex GINS protein SLD5, N-terminally processed	5E+07	2E+07	0.43	0.011
P46779	RPL28	60S ribosomal protein L28	9E+08	4E+08	0.43	0.003
Q6P2Q9	PRPF8	Pre-mRNA-processing-splicing factor 8	3E+07	1E+07	0.432	0.006
P78344	EIF4G2	Eukaryotic translation initiation factor 4 gamma 2	6E+07	2E+07	0.432	0.047
P11717	IGF2R	Cation-independent mannose-6-phosphate receptor	3E+07	1E+07	0.433	0.02
Q15149	PLEC	Plectin	4E+08	2E+08	0.435	0.028
Q07065	CKAP4	Cytoskeleton-associated protein 4	2E+08	7E+07	0.437	0.013
O60610	DIAPH1	Protein diaphanous homolog 1	3E+07	1E+07	0.438	0.005
Q9Y305	ACOT9	Acyl-coenzyme A thioesterase 9, mitochondrial	1E+08	6E+07	0.439	0.045
Q92616	GCN1L1	Translational activator GCN1	6E+07	3E+07	0.441	0.009
O15144	ARPC2	Actin-related protein 2/3 complex subunit 2	1E+08	5E+07	0.441	0.035
Q15021	NCAPD2	Condensin complex subunit 1	7E+07	3E+07	0.442	0.046
P78371	CCT2	T-complex protein 1 subunit beta	4E+07	2E+07	0.442	0.016
Q7Z3K3	POGZ	Pogo transposable element with ZNF domain	1E+07	6E+06	0.442	0.037
P49840	GSK3A	Glycogen synthase kinase-3 alpha	5E+07	2E+07	0.443	0.016

P13010	XRCC5	X-ray repair cross-complementing protein 5	5E+08	2E+08	0.443	0.006
P08240	SRPR	Signal recognition particle receptor subunit alpha	3E+07	1E+07	0.444	0.014
Q9BV19	C1orf50	Uncharacterized protein C1orf50	5E+07	2E+07	0.444	0.034
O75369	FLNB	Filamin-B	2E+08	7E+07	0.445	0.005
O00303	EIF3F	Eukaryotic translation initiation factor 3 subunit F	7E+07	3E+07	0.446	0.04
P27797	CALR	Calreticulin	1E+09	4E+08	0.446	0.005
P11413	G6PD	Glucose-6-phosphate 1-dehydrogenase	1E+08	6E+07	0.447	0.008
O43491	EPB41L2	Band 4.1-like protein 2	2E+08	8E+07	0.447	0.028
P00387	CYB5R3	NADH-cytochrome b5 reductase 3;NADH-cytochrome b5 reductase 3 membrane-bound form;NADH-cytochrome b5 reductase 3 soluble form	2E+08	9E+07	0.447	0.005
P35579	MYH9	Myosin-9	4E+07	2E+07	0.448	0.045
Q14671	PUM1	Pumilio homolog 1	2E+07	7E+06	0.449	0.01
Q14566	MCM6	DNA replication licensing factor MCM6	6E+07	3E+07	0.449	0.022
P07195	LDHB	L-lactate dehydrogenase B chain	4E+07	2E+07	0.449	0.003
Q10713	PMPCA	Mitochondrial-processing peptidase subunit alpha	5E+07	2E+07	0.451	9E-04
Q8N3U4	STAG2	Cohesin subunit SA-2	3E+07	1E+07	0.451	0.023
P11717	IGF2R	Cation-independent mannose-6-phosphate receptor	1E+07	7E+06	0.453	0.024
O60832	DKC1	H/ACA ribonucleoprotein complex subunit 4	8E+07	3E+07	0.454	0.041
P31689	DNAJA1	DnaJ homolog subfamily A member 1	5E+07	2E+07	0.454	0.019
Q9Y5K6	CD2AP	CD2-associated protein	4E+07	2E+07	0.455	0.014
P78527	PRKDC	DNA-dependent protein kinase catalytic subunit	2E+08	7E+07	0.455	0.008
P07602	PSAP	Prosaposin;Saposin-A;Saposin-B-Val;Saposin-B;Saposin-C;Saposin-D	2E+08	1E+08	0.456	0.038
Q9P2B2	PTGFRN	Prostaglandin F2 receptor negative regulator	5E+07	2E+07	0.456	0.04
P50570	DNM2	Dynamin-2	9E+07	4E+07	0.456	0.004
Q14839	CHD4	Chromodomain-helicase-DNA-binding protein 4	6E+07	3E+07	0.456	0.016
Q15345	LRRC41	Leucine-rich repeat-containing protein 41	5E+07	2E+07	0.457	0.014
P55196	MLLT4	Afadin	2E+07	9E+06	0.46	0.047
Q86UV5	USP48	Ubiquitin carboxyl-terminal hydrolase 48	3E+07	1E+07	0.46	0.005
P30038	ALDH4A1	Delta-1-pyrroline-5-carboxylate dehydrogenase, mitochondrial	2E+07	8E+06	0.46	0.029
P30419	NMT1	Glycylpeptide N-tetradecanoyltransferase 1	5E+07	2E+07	0.46	0.035
Q96AX1	VPS33A	Vacuolar protein sorting-associated protein 33A	3E+07	2E+07	0.462	0.016

P78344	EIF4G2	Eukaryotic translation initiation factor 4 gamma 2	8E+07	4E+07	0.464	0.003
P50990	CCT8	T-complex protein 1 subunit theta	3E+08	1E+08	0.464	0.011
Q14344	GNA13	Guanine nucleotide-binding protein subunit alpha-13	3E+07	1E+07	0.465	0.018
Q9BZE1	MRPL37	39S ribosomal protein L37, mitochondrial	5E+07	2E+07	0.466	0.035
Q6P158	DHX57	Putative ATP-dependent RNA helicase DHX57	3E+07	1E+07	0.466	0.041
Q9Y2R9	MRPS7	28S ribosomal protein S7, mitochondrial	7E+07	3E+07	0.466	0.04
P46087	NOP2	Probable 28S rRNA (cytosine(4447)-C(5))-methyltransferase	8E+07	4E+07	0.466	0.009
P09884	POLA1	DNA polymerase alpha catalytic subunit	4E+07	2E+07	0.468	0.02
O95453	PARN	Poly(A)-specific ribonuclease PARN	2E+08	7E+07	0.468	0.014
P10109	FDX1	Adrenodoxin, mitochondrial	9E+07	4E+07	0.468	0.003
Q9H1I8	ASCC2	Activating signal cointegrator 1 complex subunit 2	5E+07	2E+07	0.469	0.022
Q08211	DHX9	ATP-dependent RNA helicase A	3E+07	2E+07	0.47	0.037
Q7L014	DDX46	Probable ATP-dependent RNA helicase DDX46	4E+07	2E+07	0.47	0.049
Q9BXJ9	NAA15	N-alpha-acetyltransferase 15, NatA auxiliary subunit	1E+08	6E+07	0.47	0.01
Q7Z5K2	WAPAL	Wings apart-like protein homolog	2E+07	1E+07	0.471	0.012
P08243	ASNS	Asparagine synthetase [glutamine-hydrolyzing]	6E+07	3E+07	0.471	0.035
P55327	TPD52	Tumor protein D52	8E+07	4E+07	0.471	0.011
Q9NZM1	MYOF	Myoferlin	1E+07	7E+06	0.472	0.041
Q96KR1	ZFR	Zinc finger RNA-binding protein	2E+07	1E+07	0.473	0.019
Q9H2G2	SLK	STE20-like serine/threonine-protein kinase	8E+07	4E+07	0.474	0.018
Q7Z478	DHX29	ATP-dependent RNA helicase DHX29	2E+07	7E+06	0.474	0.031
Q13200	PSMD2	26S proteasome non-ATPase regulatory subunit 2	4E+07	2E+07	0.474	0.023
O43395	PRPF3	U4/U6 small nuclear ribonucleoprotein Prp3	8E+07	4E+07	0.475	0.042
Q9UKS6	PACSIN3	Protein kinase C and casein kinase substrate in neurons protein 3	1E+08	7E+07	0.476	5E-04
Q9NZJ4	SACS	Sacsin	1E+07	5E+06	0.477	0.048
P26639	TARS	Threonine--tRNA ligase, cytoplasmic	6E+08	3E+08	0.477	3E-04
Q14146	URB2	Unhealthy ribosome biogenesis protein 2 homolog	2E+07	8E+06	0.477	0.02
Q8TEM1	NUP210	Nuclear pore membrane glycoprotein 210	5E+07	2E+07	0.478	0.045
Q04637	EIF4G1	Eukaryotic translation initiation factor 4 gamma 1	3E+08	1E+08	0.478	0.003
Q01518	CAP1	Adenylyl cyclase-associated protein 1	2E+07	1E+07	0.478	0.038
P33991	MCM4	DNA replication licensing factor MCM4	2E+08	8E+07	0.479	0.017

P52732	KIF11	Kinesin-like protein KIF11	4E+07	2E+07	0.479	0.037
Q96F86	EDC3	Enhancer of mRNA-decapping protein 3	4E+07	2E+07	0.479	0.015
P62424	RPL7A	60S ribosomal protein L7a	3E+08	2E+08	0.481	0.016
Q15907	RAB11B	Ras-related protein Rab-11B	6E+08	3E+08	0.481	0.001
O94826	TOMM70A	Mitochondrial import receptor subunit TOM70	8E+07	4E+07	0.481	0.028
Q6L8Q7	PDE12	2,5-phosphodiesterase 12	8E+07	4E+07	0.483	0.013
P52701	MSH6	DNA mismatch repair protein Msh6	9E+07	4E+07	0.483	0.038
Q15208	STK38	Serine/threonine-protein kinase 38	3E+07	1E+07	0.484	0.016
P52732	KIF11	Kinesin-like protein KIF11	5E+07	3E+07	0.484	0.033
P16930	FAH	Fumarylacetoacetase	7E+07	3E+07	0.484	0.008
Q9Y6M9	NDUFB9	NADH dehydrogenase [ubiquinone] 1 beta subcomplex subunit 9	2E+07	9E+06	0.484	0.009
O00115	DNASE2	Deoxyribonuclease-2-alpha	3E+07	1E+07	0.484	0.029
Q14566	MCM6	DNA replication licensing factor MCM6	2E+08	1E+08	0.485	0.035
Q8WXH0	SYNE2	Nesprin-2	2E+07	9E+06	0.485	0.025
O75351	VPS4B	Vacuolar protein sorting-associated protein 4B	6E+07	3E+07	0.486	4E-04
Q14683	SMC1A	Structural maintenance of chromosomes protein 1A	1E+08	5E+07	0.486	0.044
P09972	ALDOC	Fructose-bisphosphate aldolase C	2E+07	1E+07	0.486	0.035
P13667	PDIA4	Protein disulfide-isomerase A4	2E+08	1E+08	0.488	0.01
Q00325	SLC25A3	Phosphate carrier protein, mitochondrial	3E+08	1E+08	0.488	0.005
Q8IXJ6	SIRT2	NAD-dependent protein deacetylase sirtuin-2	2E+07	1E+07	0.488	0.012
Q13085	ACACA	Acetyl-CoA carboxylase 1;Biotin carboxylase	1E+07	7E+06	0.488	0.037
P50990	CCT8	T-complex protein 1 subunit theta	3E+08	1E+08	0.489	0.011
Q86XI2	NCAPG2	Condensin-2 complex subunit G2	2E+07	7E+06	0.489	0.038
Q86U38	NOP9	Nucleolar protein 9	2E+07	1E+07	0.489	0.021
P62993	GRB2	Growth factor receptor-bound protein 2	9E+07	4E+07	0.489	0.019
Q13823	GNL2	Nucleolar GTP-binding protein 2	2E+07	1E+07	0.49	0.034
P78417	GSTO1	Glutathione S-transferase omega-1	7E+07	3E+07	0.491	0.049
Q09666	AHNAK	Neuroblast differentiation-associated protein AHNAK	5E+07	3E+07	0.491	0.02
Q9BZH6	WDR11	WD repeat-containing protein 11	4E+07	2E+07	0.491	0.019
Q9H583	HEATR1	HEAT repeat-containing protein 1;HEAT repeat-containing protein 1, N-terminally processed	3E+07	2E+07	0.491	0.013
P47897	QARS	Glutamine--tRNA ligase	5E+07	2E+07	0.492	0.01
Q96AC1	FERMT2	Fermitin family homolog 2	3E+07	2E+07	0.493	0.033
P14927	UQCRB	Cytochrome b-c1 complex subunit 7	4E+07	2E+07	0.493	0.024
Q7LBC6	KDM3B	Lysine-specific demethylase 3B	3E+07	1E+07	0.493	0.039
Q7Z4Q2	HEATR3	HEAT repeat-containing protein 3	2E+07	8E+06	0.494	0.048
Q9NYF8	BCLAF1	Bcl-2-associated transcription factor 1	1E+08	5E+07	0.494	0.004

P35241	RDX	Radixin	4E+08	2E+08	0.495	0.004
P61081	UBE2M	NEDD8-conjugating enzyme Ubc12	4E+07	2E+07	0.496	0.006
P52272	HNRNPM	Heterogeneous nuclear ribonucleoprotein M	4E+08	2E+08	0.496	0.042
P47897	QARS	Glutamine--tRNA ligase	1E+08	5E+07	0.496	0.041
P35579	MYH9	Myosin-9	4E+07	2E+07	0.497	0.004
P17480	UBTF	Nucleolar transcription factor 1	9E+07	5E+07	0.497	0.028
O43681	ASNA1	ATPase ASNA1	3E+07	2E+07	0.498	0.008

table S2. List of the candidate genes that related to neurodegenerative diseases

NO.	Gene names	Official Full Name (provided by HGNC)
1	*ELP2*	elongator acetyltransferase complex subunit 2
2	*POGZ*	pogo transposable element derived with ZNF domain
3	*TARDBP*	TAR DNA binding protein
4	*USP9X*	ubiquitin specific peptidase 9 X-linked
5	*DNAJC11*	DnaJ heat shock protein family (Hsp40) member C11
6	*PSMD2*	proteasome 26S subunit, non-ATPase 2
7	*UBE4B*	ubiquitination factor E4B
8	*USP24*	ubiquitin specific peptidase 24
9	*GRB2*	growth factor receptor bound protein 2
10	*RPL13*	ribosomal protein L13

table S3. The sequence of siRNAs used

NO.	Name	Species	Up: Sense (5'-3') Below: Antisense (5'-3')
1	*ELP2*	Homo sapiens	rGrGrArUrGrArCrGrArUrArArCrArUrArArGrATT
			rUrCrUrUrArUrGrUrUrArUrCrGrUrCrArUrCrCTT
2	*POGZ*	Homo sapiens	rGrGrUrUrArGrArCrCrArArUrUrArCrArCrUrATT
			rUrArGrUrGrUrArArUrUrGrGrUrCrUrArArCrCTT
3	*TARDBP*	Homo sapiens	rCrArArUrArGrCrArArUrArGrArCrArGrUrUrATT
			rUrArArCrUrGrUrCrUrArUrUrGrCrUrArUrUrGTT
4	*USP9X*	Homo sapiens	rGrGrArCrArArGrArArGrArArArCrUrGrUrUrATT
			rUrArArCrArGrUrUrUrCrUrUrCrUrUrGrUrCrCTT
5	*DNAJC11*	Homo sapiens	rGrGrArArGrUrUrUrGrUrCrArArUrGrArCrArATT
			rUrUrGrUrCrArUrUrGrArCrArArArCrUrUrCrCTT
6	*PSMD2*	Homo sapiens	rGrGrArUrGrUrGrGrUrArGrUrArCrArGrArArATT
			rUrUrUrCrUrGrUrArCrUrArCrCrArCrArUrCrCTT
7	*UBE4B*	Homo sapiens	rGrGrArUrArUrCrGrArUrGrGrUrGrUrCrUrCrATT
			rUrGrArGrArCrArCrCrArUrCrGrArUrArUrCrCTT
8	*USP24*	Homo sapiens	rGrGrArUrGrUrArCrGrGrArGrUrGrUrArGrArATT
			rUrUrCrUrArCrArCrUrCrCrGrUrArCrArUrCrCTT
9	*GRB2*	Homo sapiens	rGrGrArGrUrUrCrGrArGrArCrCrArArCrCrUrATT
			rUrArGrGrUrUrGrGrUrCrUrCrGrArArCrUrCrCTT
10	*RPL13*	Homo sapiens	rGrCrArGrUrUrUrCrUrArGrUrUrArArUrGrUrATT
			rUrArCrArUrUrArArCrUrArGrArArArCrUrGrCTT
11	*HNF1A*	Homo sapiens	rCrGrGrArGrGrUrGrCrGrUrGrUrCrUrArCrArATT
			rUrUrGrUrArGrArCrArCrGrCrArCrCrUrCrCrGTT
12	*Evi1*	Homo sapiens	rGrGrArUrUrUrCrUrGrUrUrGrUrGrUrUrUrArATT
			rUrUrArArArCrArCrArArArCrArGrArArArUrCrCTT
13	*HLF*	Homo sapiens	rGrArUrArGrArUrGrUrUrUrGrArCrUrUrUrArATT
			rUrUrArArArGrUrCrArArArCrArUrCrUrArUrCTT
14	*CP2*	Homo sapiens	rGrCrUrGrGrUrArCrCrUrArGrArArGrArCrArATT
			rUrUrGrUrCrUrUrCrUrArGrGrUrArCrCrArGrCTT
15	*Grb2*	Mus musculus	rGrGrUrArGrArArGrCrArGrArGrArGrUrGrUrATT
			rUrArCrArCrUrCrUrCrUrGrCrUrUrCrUrArCrCTT

table S4. Primers used in qRT-PCR

NO.	Primer name	Species	sequence (5'to3')	
1	*ELP2*	Human	Forward	CCCTGAAAAGGGTTGTTGTTACC
			Reverse	GAAGGGGAGCCATCCTGTTTA
2	*POGZ*	Human	Forward	ACCCAGTTTGTTAAGCCGACA
			Reverse	CTGGAGACTGAACAGCTAGTTG
3	*TARDBP*	Human	Forward	GGGTAACCGAAGATGAGAACG
			Reverse	CTGGGCTGTAACCGTGGAG
4	*USP9X*	Human	Forward	TCGGAGGGAATGACAACCAG
			Reverse	GGAGTTGCCGGGGAATTTTCA
5	*DNAJC11*	Human	Forward	GCCTACCGGAGGCTCTGTAT
			Reverse	TCCTCTCGAATTTCAGCAGGG
6	*PSMD2*	Human	Forward	TGCTCGTGGAACGACTAGG
			Reverse	CAGTTTGCCATAGTGTGGACG
7	*UBE4B*	Human	Forward	CTACCTCCCCAATAGGTGCAT
			Reverse	GGCGAGCTGCTGAGAGAAC
8	*USP24*	Human	Forward	TGGACGCGGAGAAGAATGATG
			Reverse	CTCGCTTGTAAGGGATGGACC
9	*GRB2*	Human	Forward	CTGGGTGGTGAAGTTCAATTCT
			Reverse	GTTCTATGTCCCGCAGGAATATC
10	*RPL13*	Human	Forward	TCAAAGCCTTCGCTAGTCTCC
			Reverse	GGCTCTTTTTGCCCGTATGC
11	*HNF1A*	Human	Forward	ATGGTCTCTGAGAAATAACTAC
			Reverse	ATCTGTGACTCCAATTAGCCAG
12	*EVI1*	Human	Forward	AGTGCCCTGGAGATGAGTTG
			Reverse	TTTGAGGCTATCTGTGAAGTGC
13	*HLF*	Human	Forward	CAGCAGATCTTGCCCTTTCC
			Reverse	CTTGGCTGCCATGTTGTTCT
14	*CP2*	Human	Forward	GATGTCCTTGCATTGCCCAT
			Reverse	GAGAGGTAGCAGCACAAAGC
15	*Grb2*	Mouse	Forward	AAATGCTCAGCAAACAGCGG
			Reverse	TGAAGTGCTGCACATCATTTC
16	*Gapdh*	Mouse	Forward	AGCCTCGTCCCGTAGACAAAA
			Reverse	TGGCAACAATCTCCACTTTGC
17	*GAPDH*	Human	Forward	TCCCTGCACCACCAACTGTTAG
			Reverse	GGCATGGCATGTGGTCATGAG

table S5. The hydrogen bonding interaction between GRB2 and TRKA

Receptor Residue	Ligand Residue		Distance	Type
4AOJ:ARG593	1CJ1:ASP104	4AOJ:ARG593:HH21 - 1CJ1:ASP104:OD2	2.3826	Conventional
4AOJ:GLY623	1CJ1:TRP121	4AOJ:GLY623:HN - 1CJ1:TRP121:O	2.6321	Conventional
4AOJ:GLN660	1CJ1:GLU71	4AOJ:GLN660:HE22 - 1CJ1:GLU71:OE2	2.1434	Conventional
4AOJ:GLY661	1CJ1:HIS107	4AOJ:GLY661:HN - 1CJ1:HIS107:O	2.6537	Conventional
4AOJ:GLN660	1CJ1:ARG67	1CJ1:ARG67:HH22 - 4AOJ:GLN660:O	2.1862	Conventional
4AOJ:VAL617	1CJ1:SER139	1CJ1:SER139:HN - 4AOJ:VAL617:O	2.0272	Conventional
4AOJ:GLY620	1CJ1:ARG142	1CJ1:ARG142:HH11 - 4AOJ:GLY620:O	1.9331	Conventional
4AOJ:HIS604	1CJ1:ARG142	1CJ1:ARG142:HH12 - 4AOJ:HIS604:O	2.0087	Conventional
4AOJ:HIS604	1CJ1:ARG142	1CJ1:ARG142:HH22 - 4AOJ:HIS604:O	2.5049	Conventional

table S6. The hydrogen bonding interaction between TRKA and GRB2-Rg3 complex

Receptor Residue	Ligand Residue		Distance	Type
4AOJ:ARG602	1CJ1:ASP133	4AOJ:ARG602:HH22 - 1CJ1:ASP133:O	2.3514	Conventional
4AOJ:ARG692	1CJ1:LYS124	4AOJ:ARG692:HH22 - 1CJ1:LYS124:O	2.737	Conventional
4AOJ:LYS725	1CJ1:ASP133	4AOJ:LYS725:HZ1 - 1CJ1:ASP133:O	1.9678	Conventional
4AOJ:LYS725	1CJ1:SER137	4AOJ:LYS725:HZ2 - 1CJ1:SER137:OG	1.8934	Conventional
4AOJ:GLN726	1CJ1:GLU130	4AOJ:GLN726:HE22 - 1CJ1:GLU130:O	2.6166	Conventional
4AOJ:GLY613	1CJ1:ARG78	1CJ1:ARG78:HH12 - 4AOJ:GLY613:O	2.6191	Conventional
4AOJ:GLY613	1CJ1:ARG78	1CJ1:ARG78:HH22 - 4AOJ:GLY613:O	2.51	Conventional
4AOJ:ASP674	1CJ1:TYR118	1CJ1:TYR118:HH - 4AOJ:ASP674:OD2	2.1192	Conventional
4AOJ:ASN733	1CJ1:ASN126	1CJ1:ASN126:HN - 4AOJ:ASN733:OD1	2.0976	Conventional
4AOJ:ASP674	1CJ1:LEU128	1CJ1:LEU128:HN - 4AOJ:ASP674:OD1	2.2291	Conventional
4AOJ:GLN730	1CJ1:TYR134	1CJ1:TYR134:HH - 4AOJ:GLN730:O	2.7724	Conventional

table S7. Prediction of *CRLS1* transcription factor

Scanning sequence ID: hg38_ncbiRefSeq_NM_001323562.1		
matrix identifier	**position core match matrix match sequence (always the (+)-strand is shown) (strand)**	
V$HNF1_C	128 (-) 0.874 0.878 ctgttcatttaTTGACt	*HNF1A*
V$EVI1_04	655 (+) 0.931 0.849 ggataaaacTAGATt	*Evi-1*
V$HLF_01	1319 (-) 1.000 0.931 attctGTAAC	*HLF*
V$CP2_01	1959 (-) 1.000 0.988 CTGGGtggtgc	*CP2*

table S8. Probes used in EMSA

Name	Primer sequence (5'to3')		Modification	
EVI1	Forward	aaagcctggataaaacTAGATtaccat	5'-Biotin	3'-Biotin
	Reverse	atggtaATCTAgttttatccaggcttt	5'-Biotin	3'-Biotin
EVI1-wt	Forward	aaagcctggataaaacTAGATtaccat		
	Reverse	atggtaATCTAgttttatccaggcttt		
EVI1-mut	Forward	aaagcctggataaaacGTTAAtaccat		
	Reverse	atggtaTTAACgttttatccaggcttt		

table S9. Primers used in ChIP assays

Name	Primer sequence (5'to3')	
EVI1	Forward	AGTGAAGAGCTCAGGTAATGGTG
	Reverse	TGCCTCTAATCCTTGGCACTG
HNF1A	Forward	ATTTTGGTTTCCTCTGCCCCC
	Reverse	CTGGCATTTTGGCCTGAAAGA